2013-06

Development of a cross-flow fan rotor for vertical take-off and landing aircraft

Martin, Michael J.

Monterey, California: Naval Postgraduate School

NAVAL POSTGRADUATE SCHOOL

MONTEREY, CALIFORNIA

THESIS

DEVELOPMENT OF A CROSS-FLOW FAN ROTOR FOR VERTICAL TAKE-OFF AND LANDING AIRCRAFT

by

Michael J. Martin

June 2013

Thesis Advisor: Garth V. Hobson
Second Reader: Anthony J. Gannon

Approved for public release; distribution is unlimited

THIS PAGE INTENTIONALLY LEFT BLANK

REPORT DOCUMENTATION PAGE			Form Approved OMB No. 0704–0188
Public reporting burden for this collection of information is estimated to average 1 hour per response, including the time for reviewing instruction, searching existing data sources, gathering and maintaining the data needed, and completing and reviewing the collection of information. Send comments regarding this burden estimate or any other aspect of this collection of information, including suggestions for reducing this burden, to Washington headquarters Services, Directorate for Information Operations and Reports, 1215 Jefferson Davis Highway, Suite 1204, Arlington, VA 22202–4302, and to the Office of Management and Budget, Paperwork Reduction Project (0704–0188) Washington, DC 20503.			
1. AGENCY USE ONLY ***(Leave blank)***	**2. REPORT DATE** June 2013	**3. REPORT TYPE AND DATES COVERED** Master's Thesis	
4. TITLE AND SUBTITLE DEVELOPMENT OF A CROSS-FLOW FAN ROTOR FOR VERTICAL TAKE-OFF AND LANDING AIRCRAFT		**5. FUNDING NUMBERS**	
6. AUTHOR(S) Michael J. Martin			
7. PERFORMING ORGANIZATION NAME(S) AND ADDRESS(ES) Naval Postgraduate School Monterey, CA 93943–5000		**8. PERFORMING ORGANIZATION REPORT NUMBER**	
9. SPONSORING /MONITORING AGENCY NAME(S) AND ADDRESS(ES) TDSI-National University of Singapore 21 Lower Kent Ridge Road Singapore, 119077		**10. SPONSORING/MONITORING AGENCY REPORT NUMBER**	
11. SUPPLEMENTARY NOTES The views expressed in this thesis are those of the author and do not reflect the official policy or position of the Department of Defense or the U.S. government. IRB protocol number ____N/A____.			
12a. DISTRIBUTION / AVAILABILITY STATEMENT Approved for public release; distribution is unlimited		**12b. DISTRIBUTION CODE** A	

13. ABSTRACT (maximum 200 words)

This study determined the optimum number of blades on a 4-inch diameter cross-flow fan rotor such that the rotor produced a thrust-to-weight ratio over one, which will make vertical take-off possible. The commercial computational fluid dynamics software ANSYS CFX, along with the commercial computer-aided design software SolidWorks, was used to model and perform a parametric study on the number of rotor blades. This parametric study focused on the thrust output, power requirement, and efficiency of each design in order to determine the optimum number of blades at 8,000 RPM. After the analytical study was complete, working models of three different rotors were fabricated and tested to validate the results found using ANSYS CFX. The experimental and analytical models were successfully compared at speeds ranging from 4,000 to 7,000 RPM.

14. SUBJECT TERMS Vertical take-off, vertical take-off and landing (VTOL), cross-flow fan (CFF)			**15. NUMBER OF PAGES** 73
			16. PRICE CODE
17. SECURITY CLASSIFICATION OF REPORT Unclassified	**18. SECURITY CLASSIFICATION OF THIS PAGE** Unclassified	**19. SECURITY CLASSIFICATION OF ABSTRACT** Unclassified	**20. LIMITATION OF ABSTRACT** UU

NSN 7540–01–280–5500 Standard Form 298 (Rev. 2–89)
Prescribed by ANSI Std. 239–18

THIS PAGE INTENTIONALLY LEFT BLANK

Approved for public release; distribution is unlimited

DEVELOPMENT OF A CROSS-FLOW FAN ROTOR FOR VERTICAL TAKE-OFF AND LANDING AIRCRAFT

Michael J. Martin
Ensign, United States Navy
B.S., United States Naval Academy, 2012

Submitted in partial fulfillment of the
requirements for the degree of

MASTER OF SCIENCE IN MECHANICAL ENGINEERING

from the

NAVAL POSTGRADUATE SCHOOL
June 2013

Author: Michael J. Martin

Approved by: Garth V. Hobson
Thesis Advisor

Anthony J. Gannon
Second Reader

Knox T. Millsaps
Chair, Department of Mechanical and Aerospace Engineering

THIS PAGE INTENTIONALLY LEFT BLANK

ABSTRACT

This study determined the optimum number of blades on a 4-inch diameter cross-flow fan rotor such that the rotor produced a thrust-to-weight ratio over one, which will make vertical take-off possible. The commercial computational fluid dynamics software ANSYS CFX, along with the commercial computer-aided design software SolidWorks, was used to model and perform a parametric study on the number of rotor blades. This parametric study focused on the thrust output, power requirement, and efficiency of each design in order to determine the optimum number of blades at 8,000 RPM. After the analytical study was complete, working models of three different rotors were fabricated and tested to validate the results found using ANSYS CFX. The experimental and analytical models were successfully compared at speeds ranging from 4,000 to 7,000 RPM.

THIS PAGE INTENTIONALLY LEFT BLANK

TABLE OF CONTENTS

THIS PAGE INTENTIONALLY LEFT BLANK

LIST OF FIGURES

THIS PAGE INTENTIONALLY LEFT BLANK

LIST OF TABLES

THIS PAGE INTENTIONALLY LEFT BLANK

LIST OF ACRONYMS AND ABBREVIATIONS

VTOL	Vertical take-off and landing
CFF	Cross-flow fan
UAV	Unmanned aerial vehicle
DoD	Department of Defense
HVAC	Heating, ventilation, and air conditioning
CFD	Computational fluid dynamics
CNC	Computer numerical control
Pre-preg	Pre-impregnated

THIS PAGE INTENTIONALLY LEFT BLANK

ACKNOWLEDGMENTS

I would like to express my appreciation and thanks to the following people:

Professor Garth Hobson for his guidance, patience, and genuine enthusiasm for this study.

Professor Anthony Gannon for his encouragement and willingness to share his extensive knowledge of CFD.

Chris Clay for his patience, expertise, and willingness to teach in every aspect of the CFF fabrication.

THIS PAGE INTENTIONALLY LEFT BLANK

I. INTRODUCTION

A. OVERVIEW

The concept of a vertical take-off and landing (VTOL) aircraft was first developed in the first half of the twentieth century, and the technology has been evolving ever since. VTOL aircraft have significant advantages when compared to conventional airplanes, namely that they can operate in confined environments without a conventional runway. There are a variety of propulsion methods for VTOL aircraft, including directional jet engines and rotor systems. A cross-flow fan (CFF), or a system of cross-flow fans, is another method of propulsion that has been considered for smaller aircraft, including unmanned aerial vehicles (UAVs) as proposed by Kummer and Dang [1]. CFF technology is relatively new in the aviation industry, but it has the potential to provide VTOL capabilities to UAVs used for a variety of missions in the United States military.

B. BACKGROUND

CFF technology has been used in various applications, but has not been widely used in the aerospace industry. First developed over 100 years ago, the CFF is commonly used in the heating, ventilation, and air conditioning (HVAC) industry. A commercial off-the-shelf CFF is shown in Figure 1.

Figure 1. A commercial-off-the-shelf cross-flow fan.

In the last decade there was an initiative to adapt this technology for use in the aviation industry to power aircraft. The technology is not directly transferable from a HVAC application to an aerospace application, but the scientific concept remains the same. The air is drawn in through the inlet at the top of Figure 1 and as the fan turns, the air is directed through the outlet on the bottom of the figure. In an aerospace application, the air that is directed through the outlet would be used as thrust, which is typically controlled using some type of deflector or a pivoting duct.

Unlike industrial applications, the primary objective for any aerospace application is a high thrust-to-weight ratio. For most industrial applications in which weight is not a design consideration, CFFs are manufactured out of aluminum and powered by an electric motor. To minimize the weight, the entire CFF, excluding the electric motor, is fabricated from carbon fiber. Carbon fiber is an order of magnitude stronger than aluminum, while it weighs about half as much. The thrust must be maximized in order to counteract the weight of the aircraft and produce lift during take-off. The thrust is maximized by optimizing the design of the rotor using design variables such as the number of blades, the shape of the blades and the size of the rotor.

Propulsive Wing is an American company that researches and markets CFF powered UAVs. They manufactured an aircraft composed of a very thick wing with a CFF embedded in the aft section for propulsion, which is shown in Figure 2.

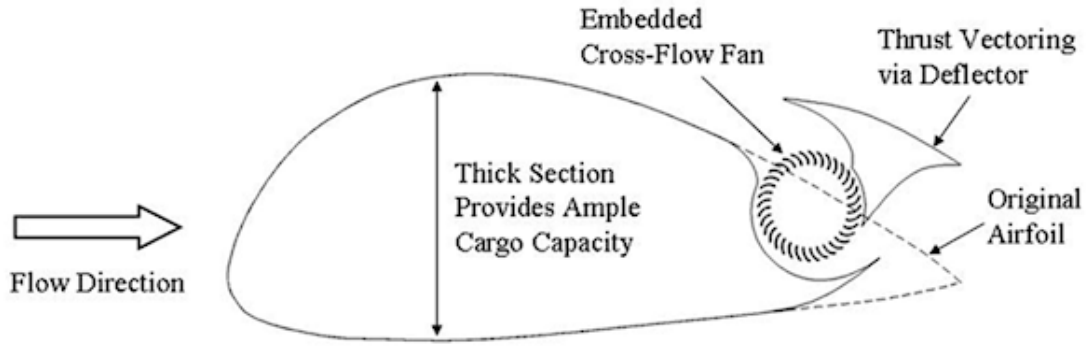

Figure 2. A schematic of the original Propulsive Wing. From [2].

In Figure 2, the air enters the embedded CFF and is then directed out of the exhaust using a deflector. The original Propulsive Wing design, shown in Figure 2, was inherently unstable and unreliable in flight. To combat this problem the company added a protruding wing on the aft of the aircraft for increased stability [2]. Propulsive Wing has successfully conducted flight tests with this improved design, which is powered by the same CFF as the original design [2]. However, it does not have a VTOL capability because the thrust-to-weight ratio of the CFF is not high enough for vertical take-off.

The goal of this thesis was to optimize a CFF rotor such that it maximized the thrust-to-weight ratio to enable vertical take-off. The CFF rotor used was similar to the one used in the Propulsive Wing aircraft. The 4-inch rotor was contained in a housing based on a CFF housing designed by Delagrange [3] in 2012. Delagrange's housing was designed to maximize the thrust produced by a 3-inch rotor and the housing in this thesis is simply scaled up to fit a 4-inch rotor. The blade profiles were the same ones used by Propulsive Wing and the number of blades was varied to optimize thrust, efficiency, and power. This optimization was first done using ANSYS CFX and then the models were experimentally tested in an attempt to validate the computational results.

THIS PAGE INTENTIONALLY LEFT BLANK

II. PARAMETRIC STUDY OF CROSS-FLOW FAN BLADE COUNT

A. OVERVIEW

An analytical study using commercial computational fluid dynamics (CFD) software was done on the CFF rotor in order to optimize the number of blades. Rotors with 16, 20, 24, 26, 28, 30, 32, and 34 blades were analyzed in ANSYS CFX at speeds ranging from 4,000–8,000 RPM for thrust, power consumption, and efficiency in order to find the optimum design. Separate models of the CFF rotor and the housing were first created in SolidWorks by sketching the side profiles and then extruding each profile 1 mm. These models were then imported separately into ANSYS CFX and combined into one model to complete a two-dimensional CFD analysis on the system. The housing was set to be stationary and the CFF rotor was free to rotate about its axis, which made the meshing of the model critical. The interface between the rotor and the housing had to be the same mesh spacing in order to get the same data resolution at the interface. A fine mesh of over 500,000 nodes was used in the CFD analysis of each rotor design.

B. SOLID MODELING

SolidWorks, a commercial design software, was used to create solid models of the housing and CFF rotors. The housing used for the 4-inch rotor was a scale model of the original design by Delagrange [3] for a 3-inch CFF rotor. The circular rotor had a variable number of blades with each blade trailing edge tangent to the center of the rotor. The profiles of the rotor and the housing domain were drawn in SolidWorks and then extruded 1 mm so a two-dimensional CFD analysis could be completed. Figures 3 and 4 show the SolidWorks models of the 26-bladed CFF rotor and the CFF housing domain.

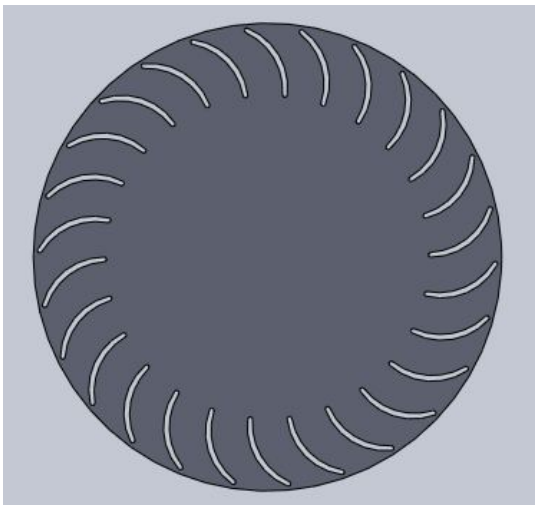

Figure 3. SolidWorks model of a 26-bladed CFF rotor.

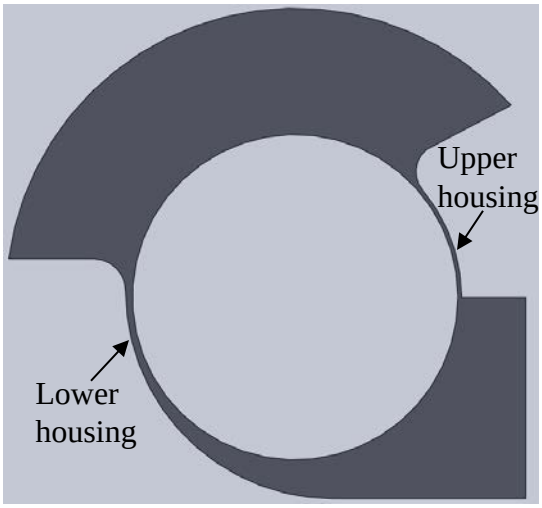

Figure 4. SolidWorks model of the CFF housing domain.

The housing domain in Figure 4 was created by drawing the upper and lower CFF housing profiles and filling the interior area between the two profiles. A 4-inch diameter hole was cut from the center of the area, as shown in Figure 4, for the CFF rotor. Complete drawings of the CFF components are provided in Appendix A. The rotor model and the housing domain were imported into ANSYS CFX as two separate files and then combined into one complete CFF model, which is shown in Figure 5.

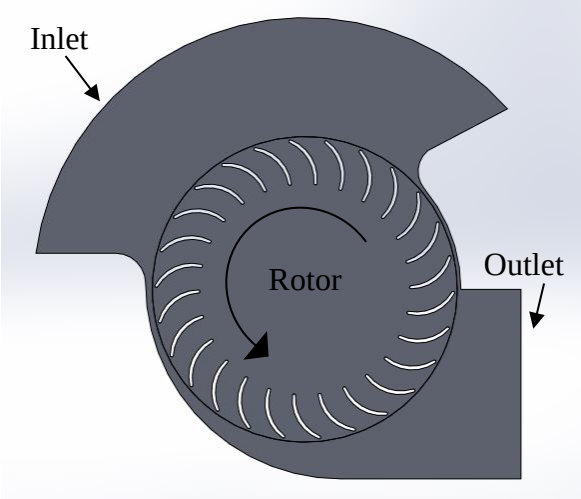

Figure 5. SolidWorks model of the 26-bladed CFF assembly.

This assembly is the complete model that was used in ANSYS CFX to optimize the number of blades on the CFF rotor. The circular arc on the top is the inlet of the CFF and the rectangular duct on the right is the outlet from which the thrust is generated.

C. MESH GENERATION AND BOUNDARY CONDITIONS

1. Mesh Generation

After the rotor and the housing models were imported from SolidWorks into ANSYS CFX, they were combined to form the assembly in Figure 5. A fine mesh was generated in ANSYS CFX for this assembly with over 500,000 nodes and 400,000 elements. A complete mesh generated for the 16-bladed CFF assembly is displayed in Figure 6.

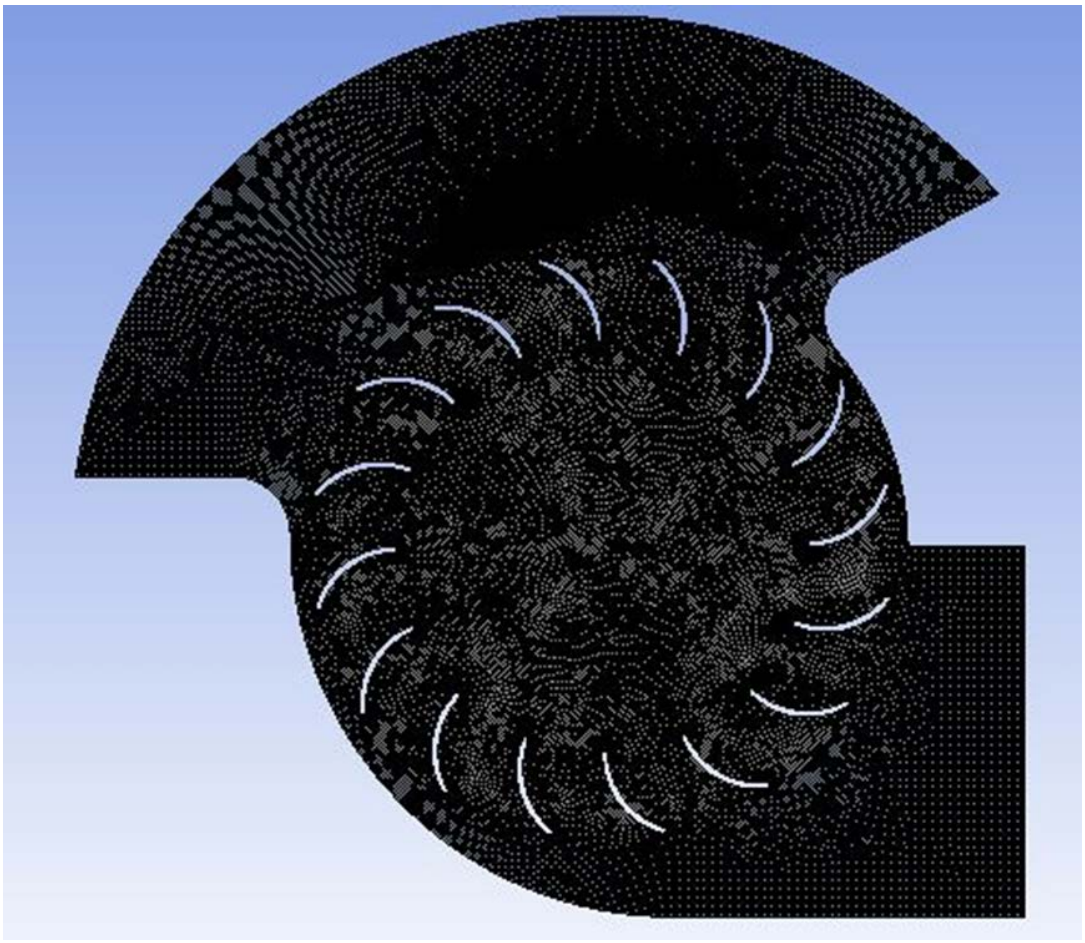

Figure 6. A fine mesh of the 26-bladed CFF assembly.

The housing was added as a frozen entity with the rotor being free to rotate. Edge sizing was used in the fluid interface between the two parts in order to match the element size between the housing and rotor. Figure 7 shows that the mesh along the interface was the same size on both the housing and the rotor.

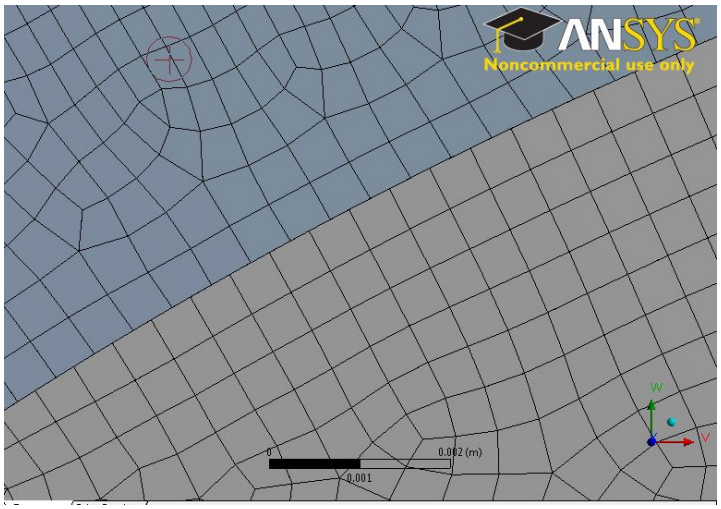

Figure 7. Edge sizing along the interface between the housing and the rotor.

The housing is on the top left of Figure 7, while the rotor is on the bottom right. This edge sizing provided continuity over the interface such that the CFD analysis was accurate throughout the CFF assembly.

2. Defining Boundary Conditions

The boundary conditions of the CFD simulation in ANSYS CFX were critical to obtaining an accurate solution. The boundaries of the CFF assembly were defined as illustrated in Figure 8.

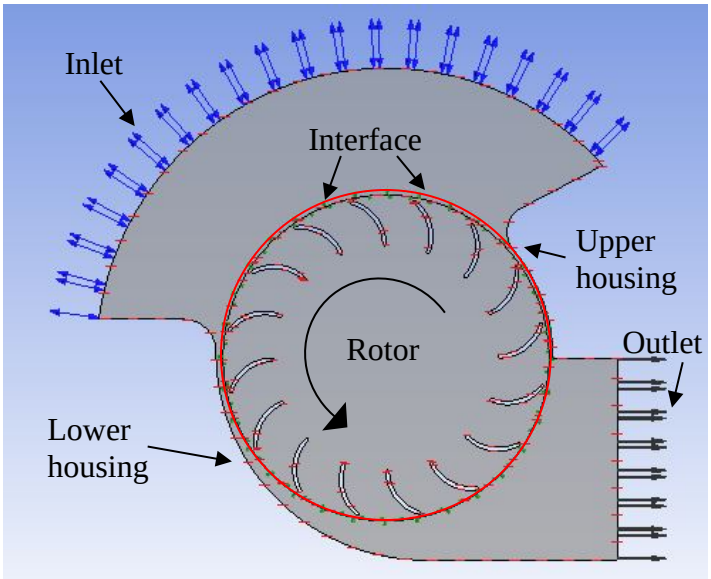

Figure 8. Boundaries of the CFF assembly.

An interface was also created between the housing and rotor so data could be smoothly transferred across the two domains. The inlet was modeled as an opening with a relative stagnation pressure of 0 Pa and the initial temperature at the inlet was specified as 288.15 K.

The total time and the time steps for each transient simulation were adjusted such that the rotor rotated one degree per time step in the counterclockwise direction for five revolutions, as it took approximately five revolutions for the solution to converge, or the mass flow rate to stabilize during the simulation [4]. Between each time step, three inner iterations were used to resolve the non-linearity in the flow field. A no slip wall condition was set for all of the wall boundaries, including each of the blades and both of the housing walls. A total-energy model and a k-Epsilon turbulence model were used in the analyses because the flow within the rotor was assumed to be turbulent. Using these conditions a transient analysis with air as an ideal gas was done on the CFF model with rotors of varying blade counts. The ANSYS CFX program solved the two-dimensional, unsteady Navier-Stokes equations for the flow through the CFF assembly. A complete description of the initial conditions and boundary conditions for the 26-bladed rotor at 7,000 RPM is given in Appendix B.

D. CFD SIMULATION

The mass flow rates at the inlet and outlet, as well as the difference in mass flow rates, were monitored at each time step to ensure that the results converged on a stable solution within five rotations of the rotor. Data collected from these CFD analyses allowed a comparison of thrust, power consumption, and efficiency for rotors with different numbers of blades at the same speed. The primary design variable was thrust, with power consumption and efficiency being secondary optimization parameters. The optimum design maximized thrust and efficiency while minimizing power consumption. In addition to optimizing the blade count of the rotor, thrust and power curves were also created for the individual rotors as a function of rotational speed. To calculate thrust and power, the rotor torque and mass flow rate at the outlet were monitored throughout the simulation and pressure and efficiency values were found using an ANSYS CFX results function calculator.

THIS PAGE INTENTIONALLY LEFT BLANK

III. CROSS-FLOW FAN FABRICATION AND EXPERIMENTAL SETUP

A. FABRICATION OF SOLIDWORKS MODELS

After the analytical model was complete, CFF assemblies were fabricated to validate the computational results. The SolidWorks drawings, which are shown in Appendix A, were used to manufacture a housing assembly and rotors of 20, 26, and 30 blades. In addition to the components used in the analytical model, there were also two housing end plates and a circular support disk in the middle of the rotor. These pieces were not of value in the computational model, but are essential for structural support in the model. A computer numerical control (CNC) router with a diamond plated bit, pictured in its enclosure in Figure 9, was used to cut the rotor end plates, the circular support disk, and the housing end plates from a carbon fiber plate.

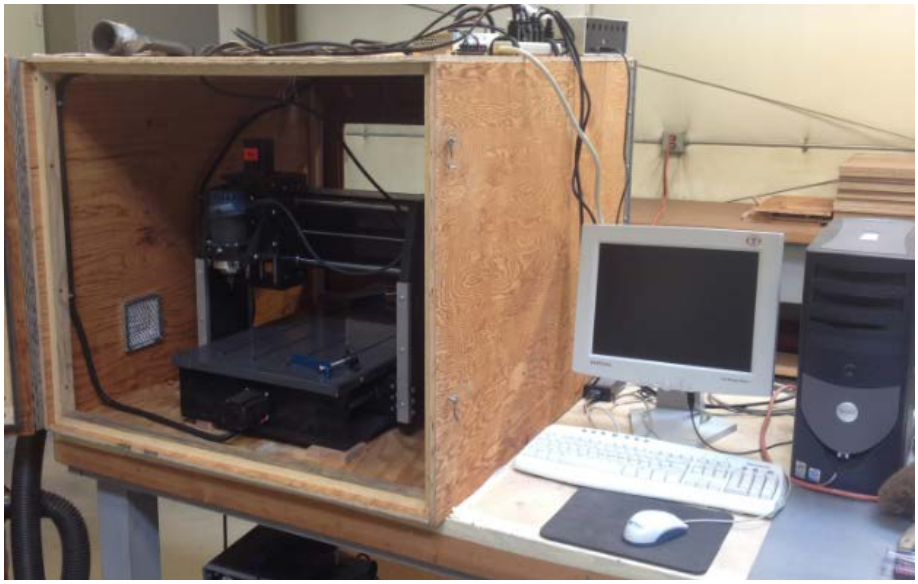

Figure 9. The CNC router used to cut the rotor and housing end plates.

The CFF blade profiles were purchased as 48-inch long pultruded carbon fiber blade sections. The pultruded carbon fiber lengths were cut into 9-inch long sections, which were later trimmed in the final assembly to be the proper length for an 8-inch long

rotor. These blades, the two rotor end plates, and the circular support disk were assembled using Loctite Hysol E-120HP epoxy to form each complete rotor, such as the 26-bladed rotor in Figure 10.

Figure 10. The complete manufactured 26-bladed rotor.

Constructing the housing profiles was a multi-stepped process. First, wooden molds of the profiles were cut using the CNC router and pressed together. These molds were mounted in a custom built aluminum jig and sanded down so the surface was even and homogenous. Several coats of an epoxy were painted on the wooden surface so that it became glossy and smooth. These complete molds are shown below in Figure 11.

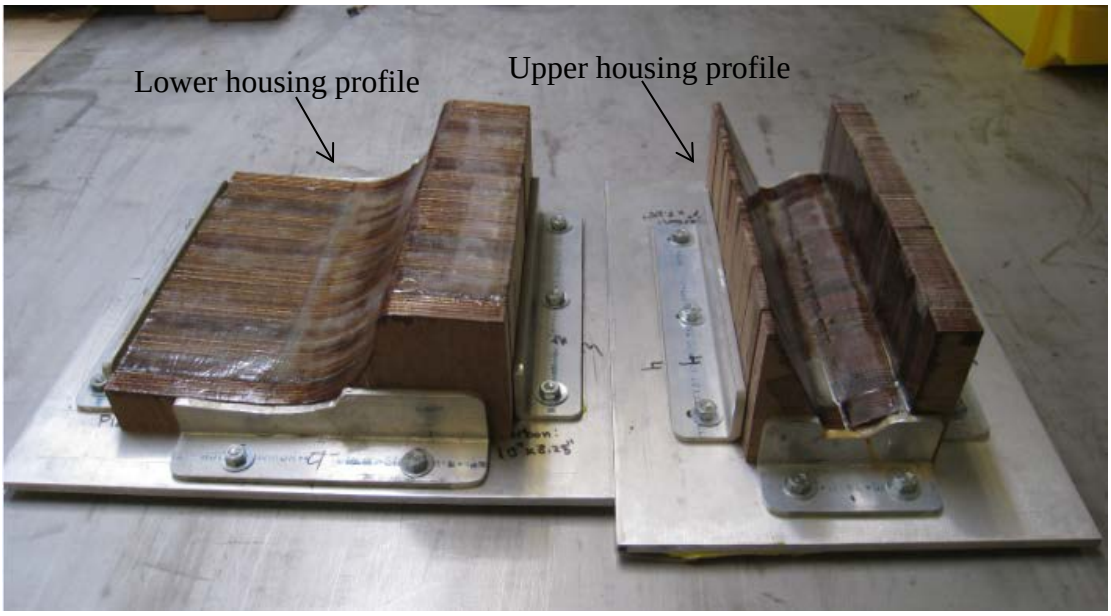

Figure 11. The molds for the lower and upper housing profiles.

Once the mold was coated with a release agent, three sheets of pre-impregnated (pre-preg) carbon fiber were layered at alternating angles for improved strength. This entire assembly was vacuum baked in an oven and these resulting carbon fiber structures were used as the housing profiles. These housing profiles were reinforced with carbon fiber stiffeners of "top-hat" sections that strengthened the housing against torsion, without adding significant weight. Once completed, the housing profiles and the housing end plates were assembled using right angled carbon fiber tabs and screws. The carbon fiber stiffeners and angled tabs are shown on the bottom housing profile in Figure 12.

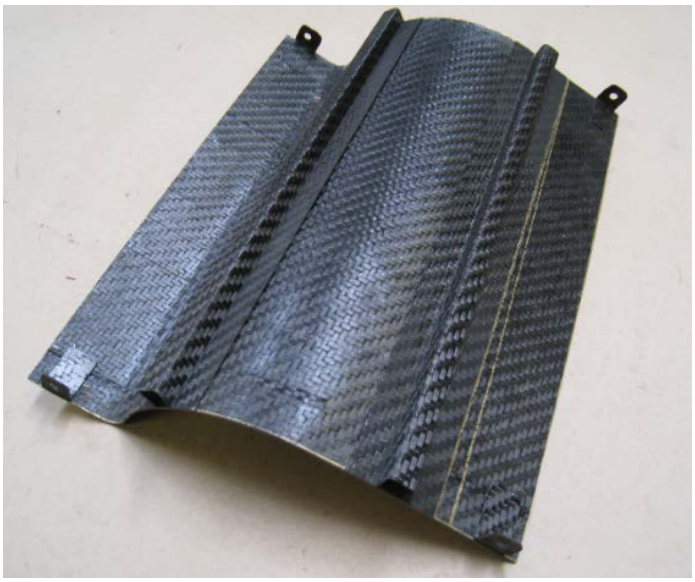

Figure 12. Stiffeners and angled tabs on the lower housing profile.

The individual components were combined to form the final assembly in Figure 13.

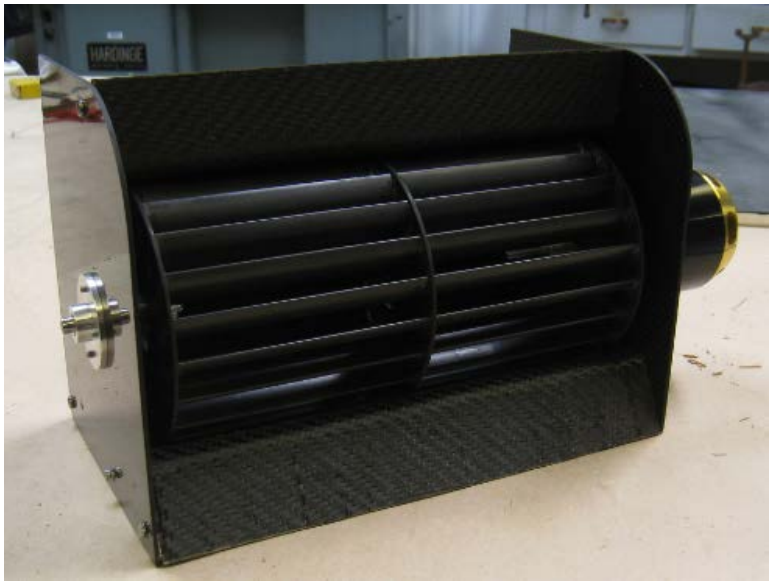

Figure 13. The final CFF assembly.

As shown in Figure 13, Aluminum bushings were manufactured for the rotor end plates and the housing end plates. These bushings provided an interface between the rotor, the housing, and the motor output shaft and allowed for the changing of the rotor while the rest of the assembly remained intact.

B. LABORATORY SETUP

1. Testing Apparatus

Each of the CFF rotors was tested in a laboratory using the experimental set-up shown in Figure 14. This consisted of the CFF assembly mounted to two aluminum brackets, a motor, a battery pack, and a controller. The testing apparatus remained constant as the 20, 26, and 30 blade rotors were all tested at different speeds.

Figure 14. The CFF experimental set-up.

As seen in Figure 14, two wooden platforms were positioned on either side of the CFF outlet. These platforms prevented the CFF from re-ingesting the air that was previously expelled from the outlet, as this could cause inaccurate thrust measurements.

The motor used to power the CFF was the Scorpion HK-5035–410KV. This electric motor had a 6-mm output shaft and was rated to operate at temperatures of 180 degrees C (356 degrees F). It had a maximum continuous power of 5,100 watts and a maximum continuous current of 105 amperes, as well as a peak power of 7,000 watts for

5 seconds and a peak current of 145 amperes for 5 seconds [5]. Scorpion Power System LTD included a controller assembly with the Scorpion HK-5035–410KV motor which was used to control the speed of the motor. This assembly was mounted in the custom built speed control console in Figure 15 for ease of use.

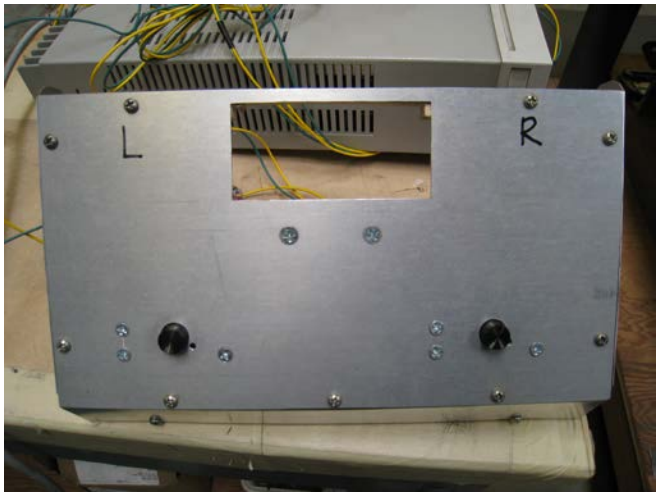

Figure 15. The speed control consoleA Type 1531-AB Strobotac stroboscope, shown in Figure 16, was used to measure the speed of the rotor.

Figure 16. The stroboscope used to monitor the rotor speed.

The desired rotor speed was set on the strobe and the motor was increased or decreased based on the apparent direction the rotor was spinning when viewed under the strobe. When the rotor appeared to be stationary, the rotor speed matched the strobe speed.

2. Data Acquisition and Instrumentation

As tests were run on the testing apparatus, there were three main parameters of interest: current to the motor, battery voltage, and force. This data allowed for the calculation of thrust generation and power consumption for each rotor design. In each trial a voltmeter was used to measure the voltage provided by the battery and an ammeter, shown in Figure 17, was used to measure the current to the motor.

Figure 17. An ammeter measuring the current to the motor.

The thrust was measured using the Adam Equipment CPWplus 15 digital scale shown in Figure 18, which was placed 10.5 inches below the CFF outlet. A sheet of aluminum was placed on top of the scale in order to ensure that all of the thrust generated by the CFF was measured by the scale.

Figure 18. The digital scale used to measure thrust.

Unlike a traditional triple beam balance, this scale had a digital display with a resolution of 5 grams, which increased the consistency and accuracy of each reading. Because this study primarily analyzed the thrust generated by various rotor designs, consistency and accuracy were important for meaningful results.

THIS PAGE INTENTIONALLY LEFT BLANK

IV. RESULTS AND DISCUSSION

A. CONVERGENCE OF ANALYTICAL RESULTS

The mass flow rates at the inlet and outlet of the CFF assembly, as well as the difference in these two mass flow rates, were monitored throughout the solution in order to ensure the ANSYS CFX solution converges in five revolutions. Figure 19 is plot of these mass flow parameters for the 16-bladed rotor at 8,000 RPM.

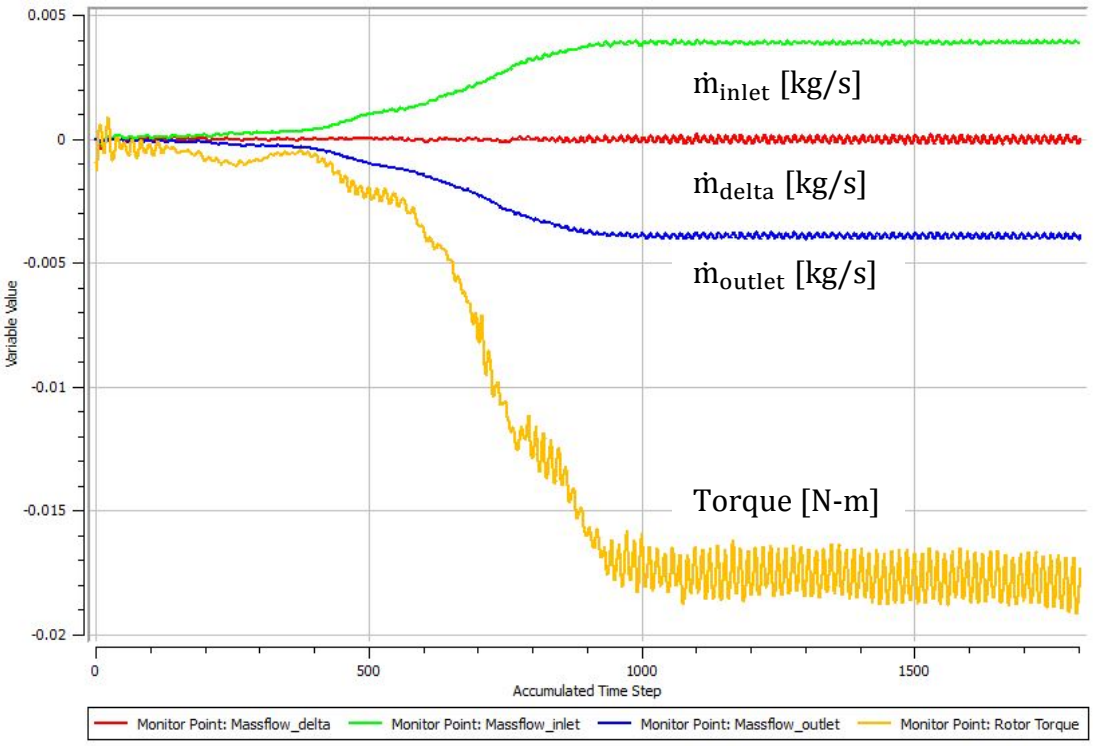

Figure 19. The mass flow rate and torque data for the 26-bladed rotor.

The green and blue data plots are the mass flow rates at the inlet and outlet, respectively, and the red and yellow data plots are the difference in mass flow rates and the rotor torque, respectively. Figure 19 shows that the data converged on a solution around 1,200 time steps, which was about 3.33 revolutions at one degree of rotation per time step. These results confirm Yu's results that the solution converged within five revolutions, or 1,800 time steps [4].

B. FLOW VISUALIZATION

The flow pattern inside the CFF assembly was analyzed within ANSYS CFX-Post. Velocity contours and velocity streamlines were plotted over the CFF in order to see where the maximum air velocities were generated and to identify recirculation zones. Figure 20 shows velocity contours generated by the 20-bladed CFF assembly at 8,000 RPM in ANYSYS CFX-Post.

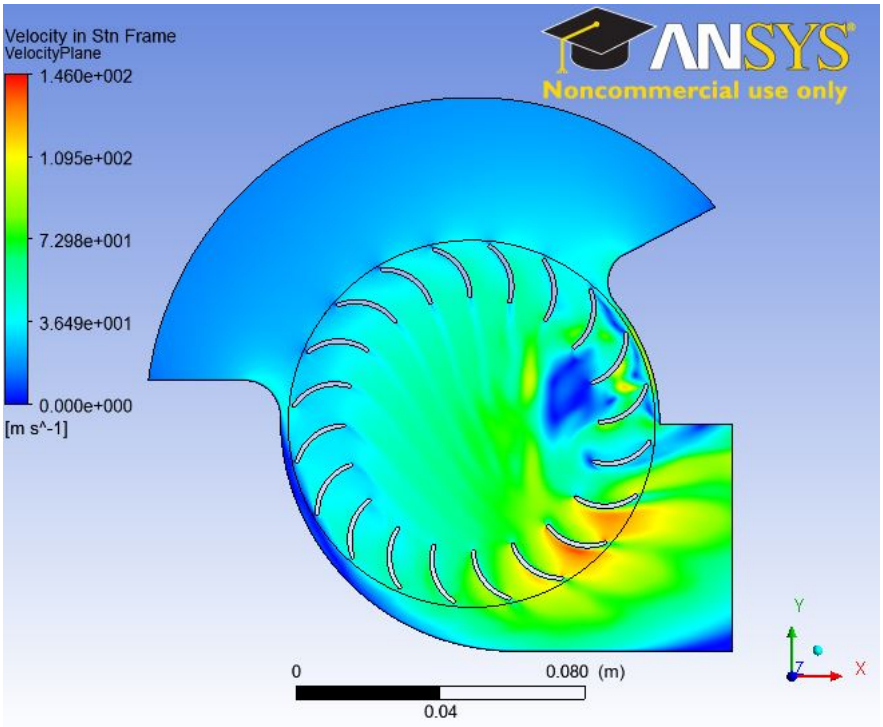

Figure 20. The velocity contour of the 20-bladed CFF.

As the blades rotate in the counter clockwise direction, the largest air velocities are seen on the suction side of the blades as they pass the outlet. The shape and size of the outlet ensured this high velocity air exits the assembly unobstructed and therefore, all of the air flowing in the horizontal direction of this model could be utilized as thrust. Velocity streamlines are also overlaid on the same CFF model in Figure 21.

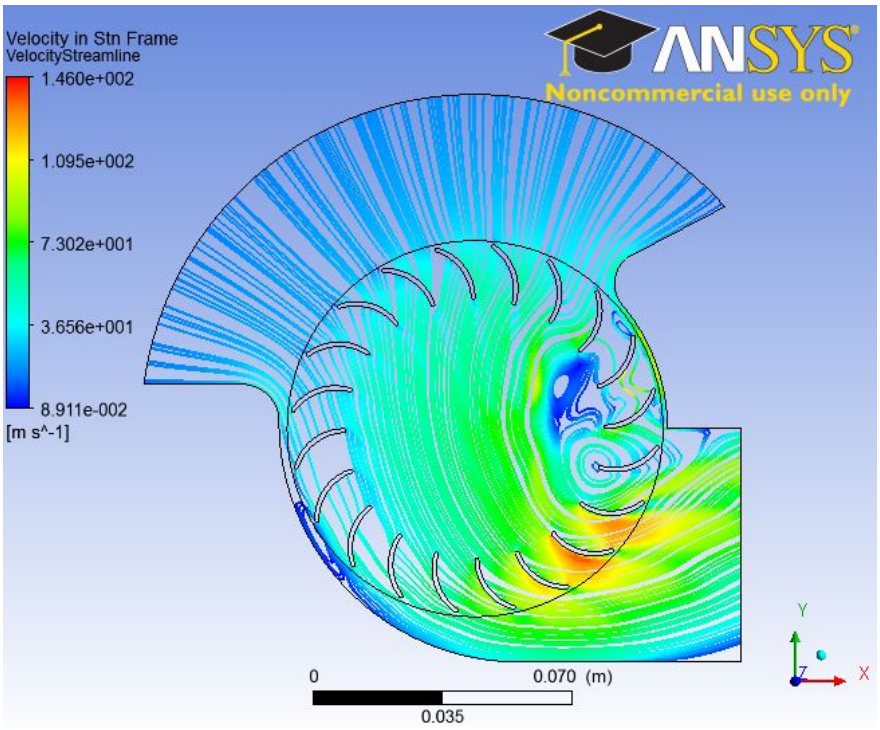

Figure 21. The velocity streamlines for the 20-bladed CFF at 8,000 RPM.

The velocity streamlines highlight two prominent recirculation regions: one to the right of the rotor center and one between the rotor and the lower housing profile. These streamlines reiterate that the high velocity air generated by the rotor was all directed out of the exhaust without obstruction.

C. ANALYTICAL RESULTS

1. Thrust

Because ANSYS CFX does not directly calculate the thrust, Equation (1) was used for thrust calculations.

$$T = \dot{m}_{exit} * V_{exit} \quad (1)$$

The thrust was calculated based on the average mass flow rate between time step 1,200 when the solution first converged and time step 1,800 at the end of the simulation. The exit velocity, which was found using the function calculator in ANSYS CFX, was the mass averaged velocity at the outlet in the X-direction.

The analytical model was used to calculate the thrust values for rotors with 16, 20, 24, 26, 28, 30, 32, and 34 blades at 8,000 RPM. These thrust values are shown in Figure 22 as a function of the number of blades.

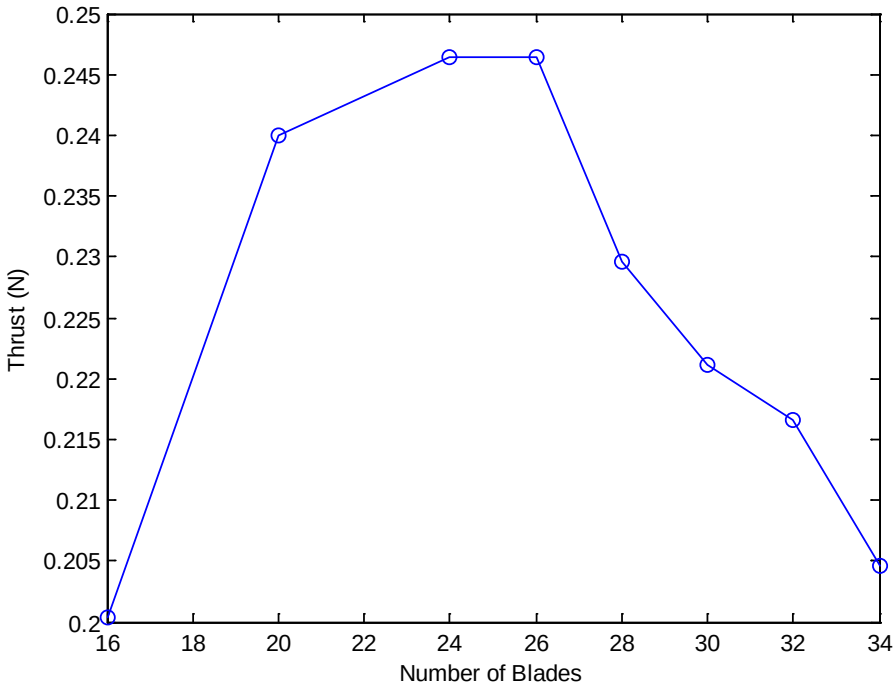

Figure 22. Thrust as a function of the number of blades at 8,000 RPM.

Because these results are for the 1 mm thick cross section, the magnitude of the thrust measurements is unimportant. The peak relative thrust is obtained with a 24 or 26-bladed rotor and there is a sharp decrease in thrust as the number of blades is decreased past 20 or increased more than 26.

2. Power

The power consumption was calculated using the rotor torque and rotor speed in Equation (2). This parameter was the amount of power required to operate the CFF rotor at a specific speed.

$$P=T_{rotor}*\omega \quad (2)$$

The rotor torque was monitored throughout each simulation and the average value between time step 1200 when the solution first converged and time step 1,800 was used in Equation (2). Figure 23 is a curve showing power consumption as a function of the number of blades at 8,000 RPM.

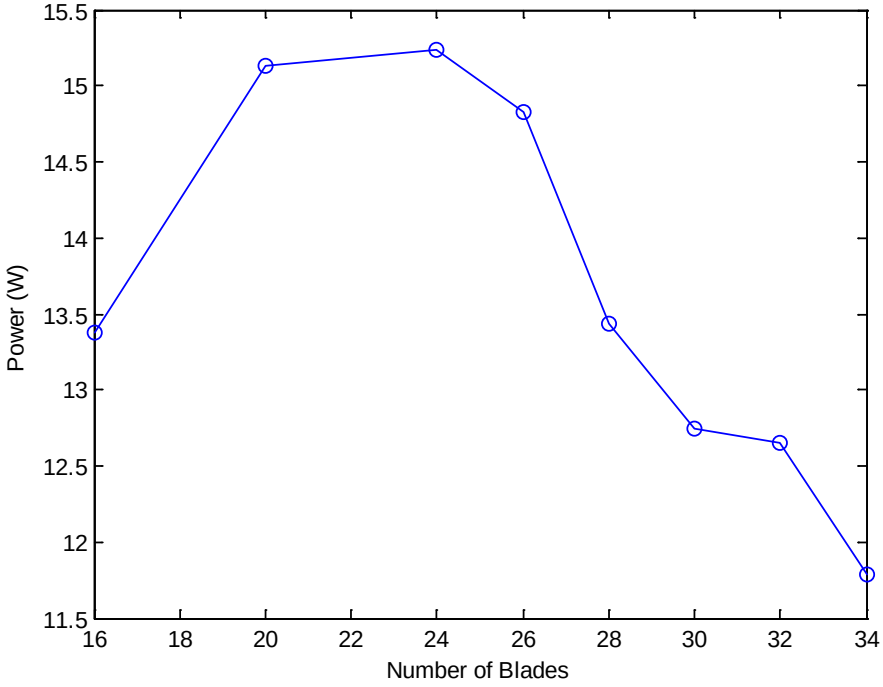

Figure 23. Power as a function of the number of blades at 8,000 RPM.

The magnitude of the power values in Figure 23 is irrelevant because the simulation was done for a 1 mm thick cross section, but the curve is significant. A 24-bladed rotor consumed the most power and the power consumption significantly decreased as the number of blades was increased beyond 24 or decreased less than 20.

3. Efficiency

In addition to thrust and power, efficiency was also calculated as a function of the number of blades. A gas compressor analysis was done on the CFF assembly in ANSYS CFX-Post in order to calculate a total-to-total isentropic efficiency. This efficiency is plotted as a function of the number of blades in Figure 24 at 8,000 RPM.

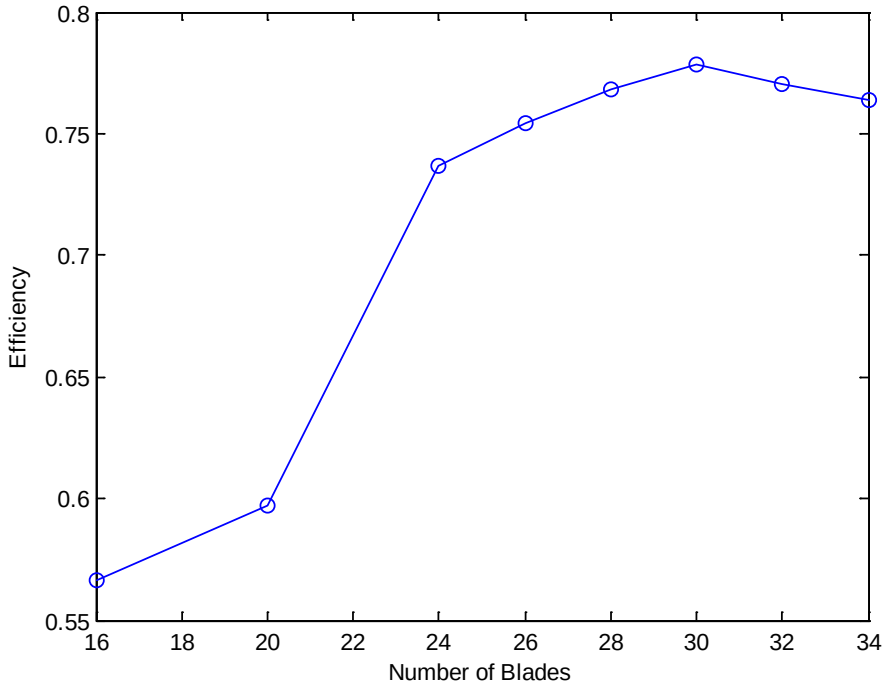

Figure 24. Analytical results for efficiency as a function of blade count.

The efficiency increased as the number of blades increased and then peaked at a 30-bladed rotor before decreasing.

D. COMPARISION OF ANALYTICAL AND EXPERIMENTAL RESULTS

1. Thrust

Rotors of 20, 26, and 30 blades were experimentally tested in order to validate the analytical results. The thrust was measured for each of the rotors at speeds of 4,000, 5,000, 6,000, and 7,000 RPM. The experimental thrust measurements were compared to the analytical thrust measurements and are presented in Figures 25–27.

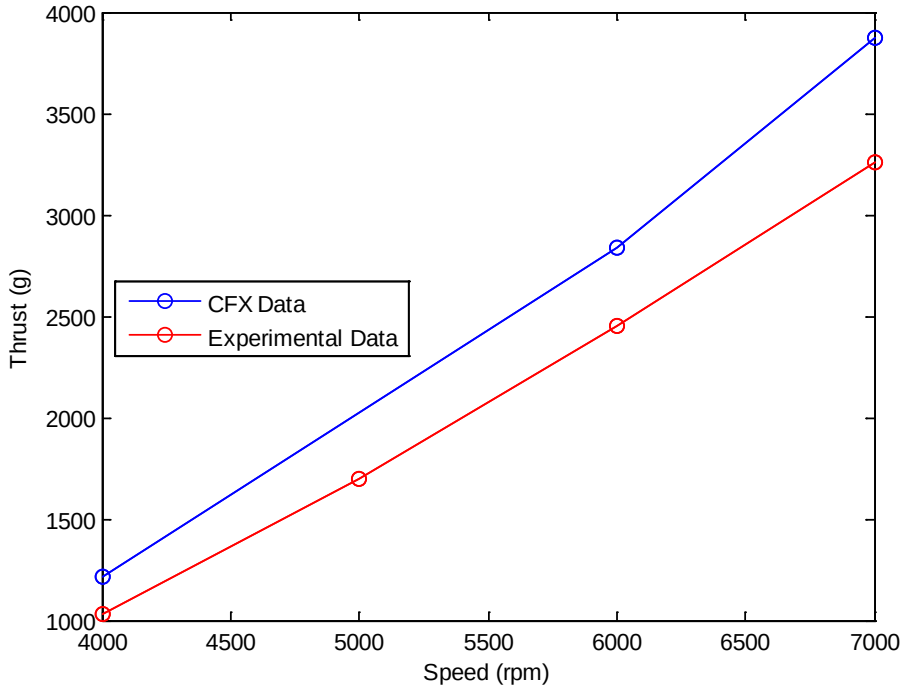

Figure 25. Experimental and analytical thrust data for the 20-bladed rotor.

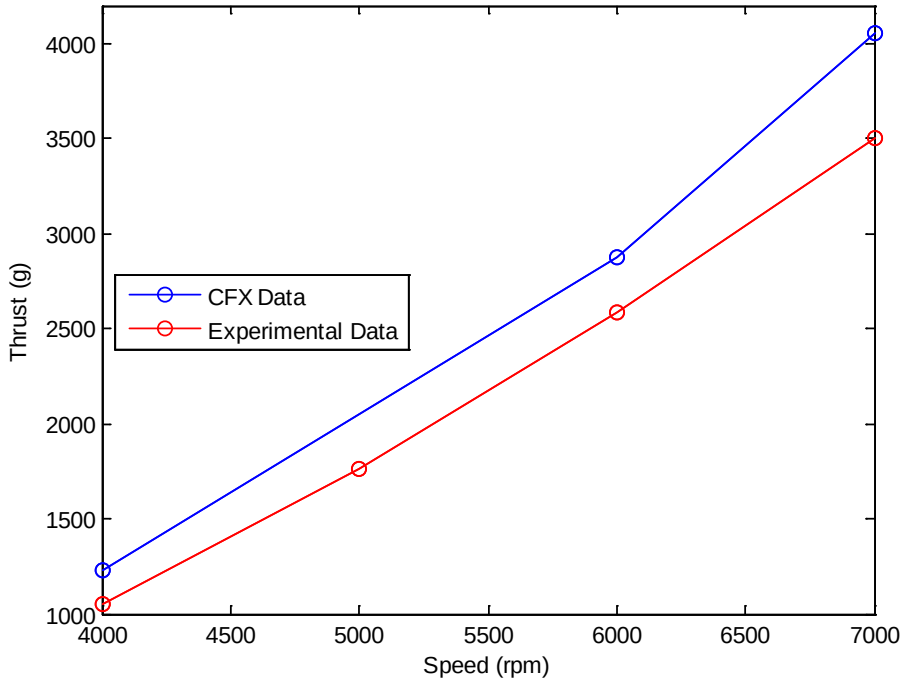

Figure 26. Experimental and analytical thrust data for the 26-bladed rotor.

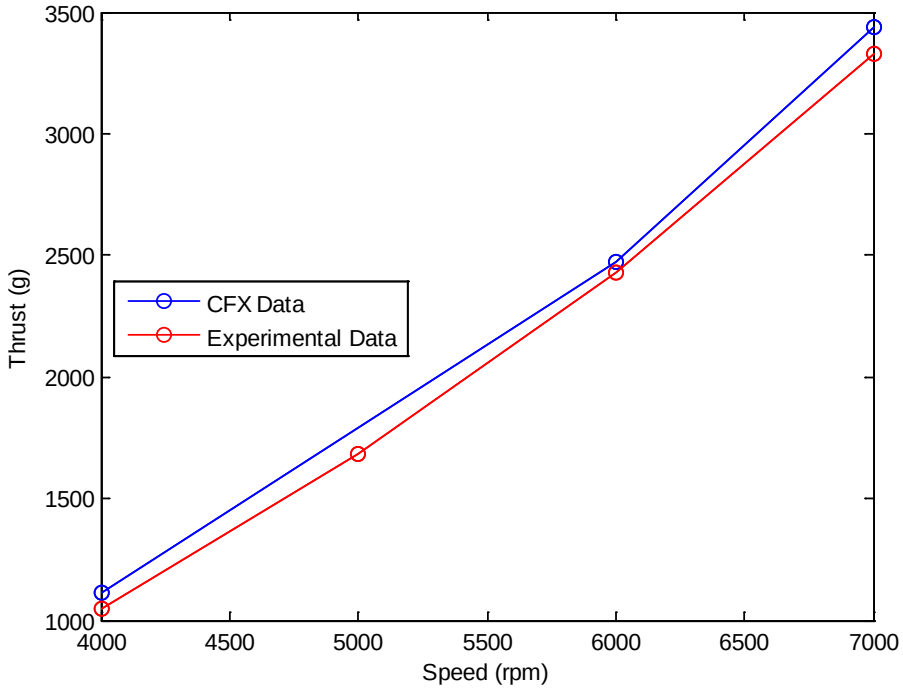

Figure 27. Experimental and analytical thrust data for the 30-bladed rotor.

The experimental thrust results were consistently lower than the analytical results. The analytical thrust results were found for the 1 mm rotor cross section and then linearly extrapolated to a 203.2-mm (8-inch) rotor cross section for comparison with the experimental rotor. However, the linear extrapolation did not account for the circular support disk in the middle of the experimental rotor span. This support disk significantly decreased the flow at the mid-span of the rotor and caused thrust generation to be non-uniform along the length of the rotor [3].

The analytical and experimental thrust measurements were also compared for different rotors at the same speed. The analytical model was used to compare thrust and power values for different rotors at 8,000 RPM, but the rotors could not experimentally reach 8,000 RPM with the Scorpion HK-5035–410KV motor. However, the relative thrust and power values remain the same regardless of speed. Figure 28 compares experimental and analytical thrust data for the different rotors at 7,000 RPM.

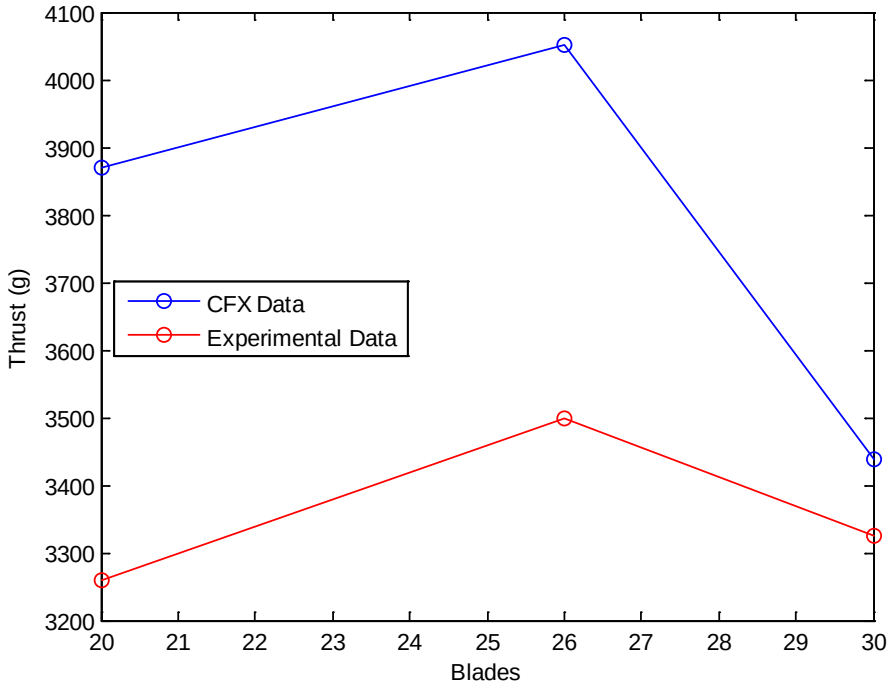

Figure 28. Experimental and analytical thrust comparison at 7,000 RPM.

The experimental thrust values confirmed the analytical prediction that the maximum thrust was achieved with a 26-bladed rotor. The analytical model predicted a peak thrust value of 4,052 g, while the fabricated rotor generated only 3,500 g of thrust. The experimental results were lower than the analytical results, which is consistent with the results in Figures 25–27.

2. Power

The power was also found experimentally and compared to the analytical power values. The experimental power was calculated using the battery voltage and the motor current in Equation (3).

$$P=V_{battery}*I_{motor} \quad (3)$$

The power curves for the 20, 26, and 30-bladed rotors at different speeds are plotted in Figures 29–31.

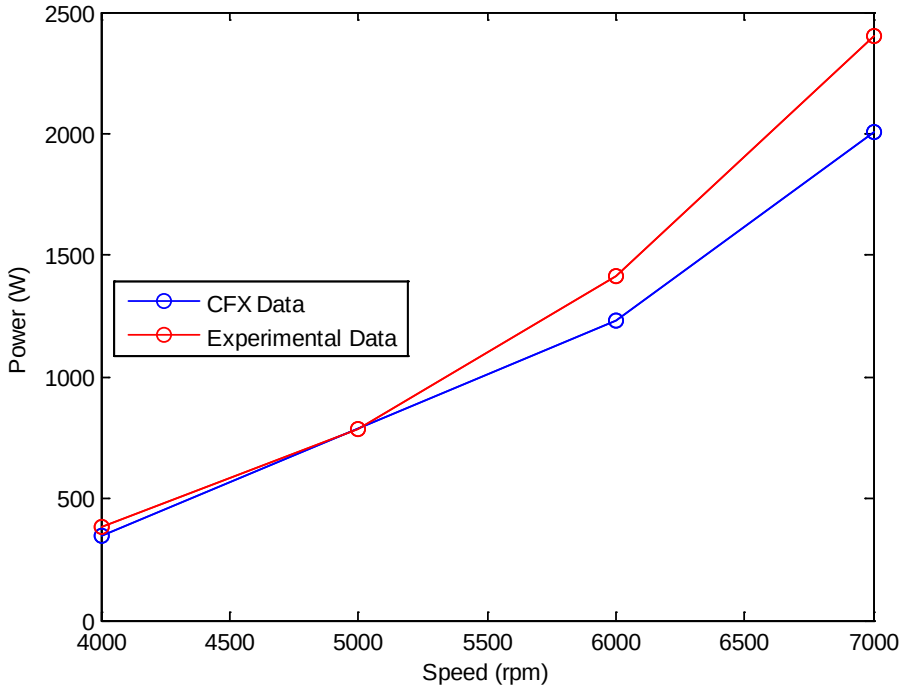

Figure 29. Power as a function of speed for a 20-bladed rotor.

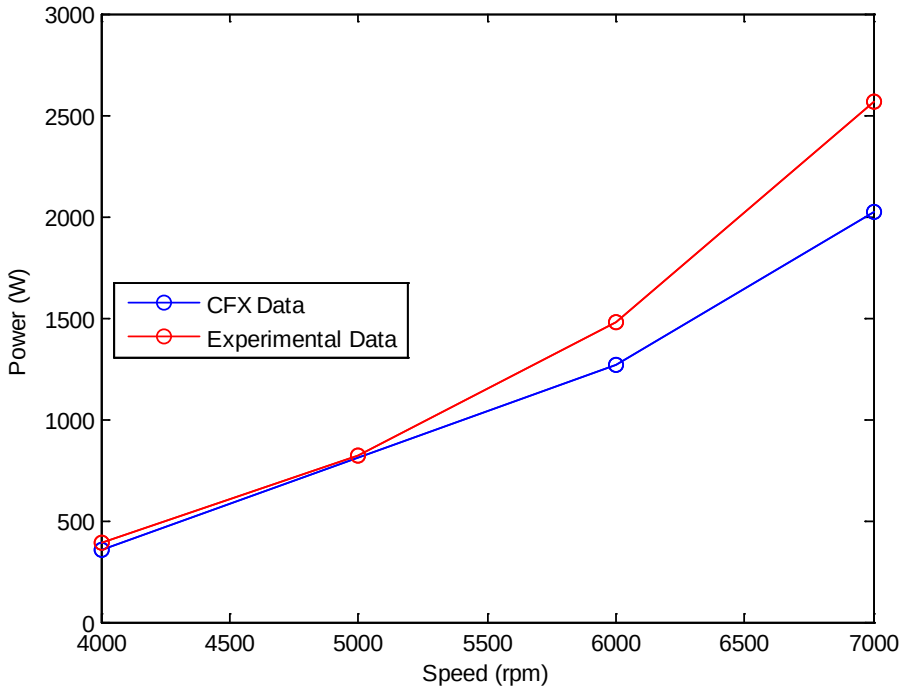

Figure 30. Power as a function of speed for a 26-bladed rotor.

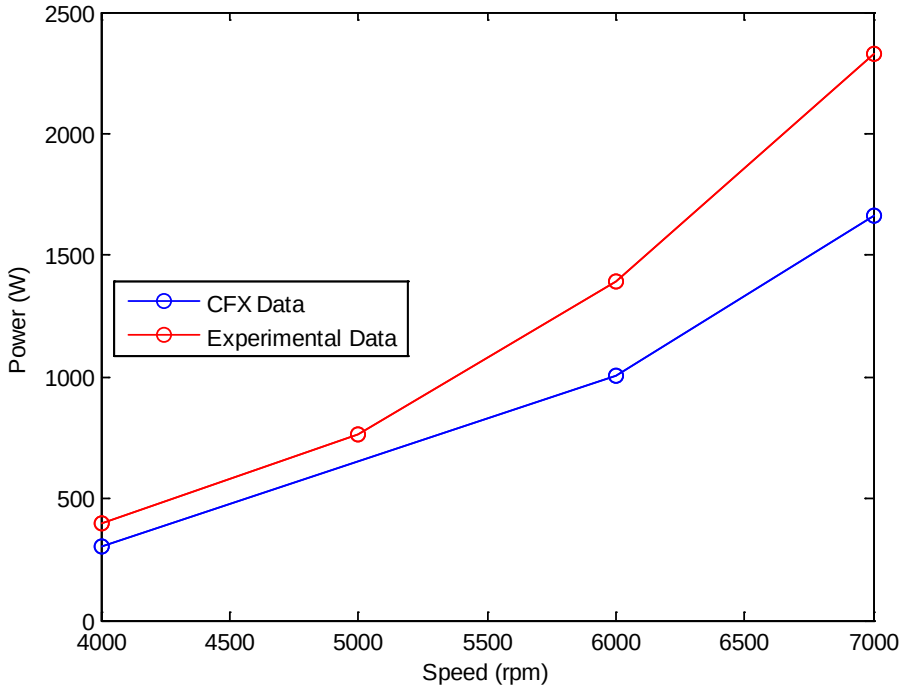

Figure 31. Power as a function of speed for a 30-bladed rotor.

The relative power curves predicted by the analytical model were confirmed with the experimental power measurements. The analytical power predictions were consistently lower than the experimentally measured power values because there were significant electrical losses that were unaccounted for in the analytical model. The power values predicted for each rotor were relatively accurate at low speeds, but the two curves diverged as the speed is increased. This divergence is caused by an increase in electrical losses as the speed of the motor increased.

The experimental and analytical power values were also compared for the different rotors at 7,000 RPM in Figure 32.

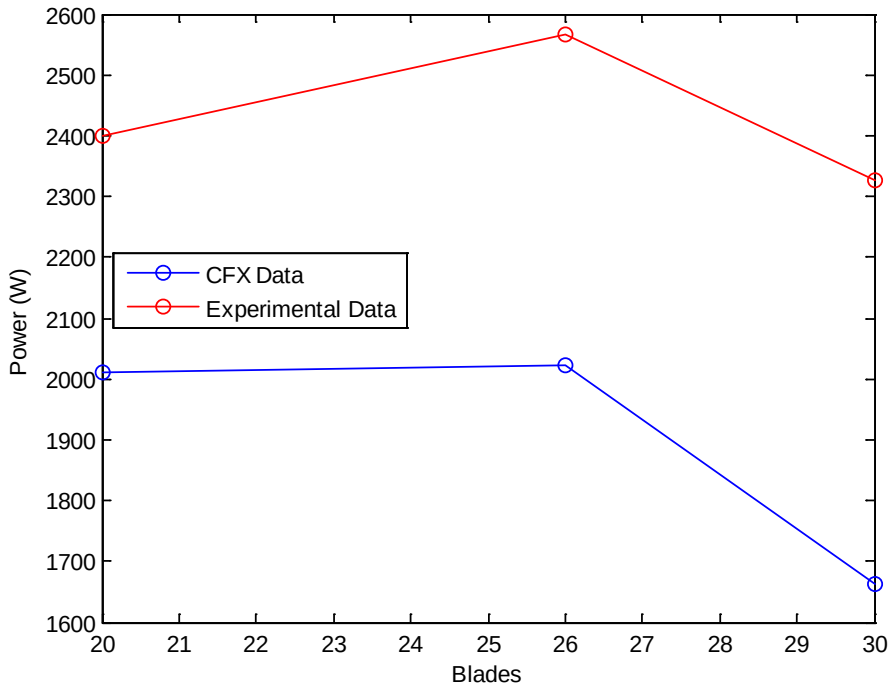

Figure 32. Experimental and analytical power data at 7,000 RPM.

The analytical model predicted a peak power consumption of 2,022 W for the 26-bladed rotor, while the fabricated model consumed 2,566 W of power. The analytical predictions for the power values were lower than the experimental data, but the relative trend between the 20, 26, and 30-bladed rotors was the same. The experimental and analytical data both demonstrated that the 26-bladed rotor consumed the most power. However, the experimental data showed a significant increase in power consumption between the 20 and 26-bladed rotors, while the analytical model predicted a modest power increase between these two designs.

V. CONCLUSIONS

A. OPTIMUM DESIGN

The analytical models were used to determine the optimum rotor design that maximized thrust, while also minimized power consumption and maximized efficiency. Peak thrust was generated by the 24 and 26-bladed rotors, with a slight thrust decrease when the blade count was decreased to 20 blades and a sharp thrust decrease at 28 blades. Power consumption peaked with a 24-bladed rotor and significantly decreased with a 26-bladed rotor, while the efficiency increased until the blade count reached 30 blades. There was conclusive evidence in the analytical model, which was experimentally validated, that the optimum number of blades for the 4-inch rotor was 26.

B. THRUST-TO-WEIGHT RATIO

The ultimate goal of this study on CFF rotors was to design a rotor that could produce a thrust-to-weight ratio over one such that vertical take-off is possible. Table 1 shows the three fabricated rotors with the corresponding experimental thrust measurements at 7,000 RPM, the assembled rotor masses, and thrust-to-weight ratios. Each assembled rotor mass included the mass of the rotor, the housing, the battery, as well as the motor and its components.

Table 1. Experimental thrust-to-weight ratios for different rotor designs.

Rotor	Assembled Rotor Mass (kg)	Thrust (kg)	Thrust-to-Weight Ratio
20 Blades	2.145	3.260	1.520
26 Blades	2.160	3.500	1.620
30 Blades	2.185	3.325	1.522

The thrust-to-weight ratio of the 26-bladed rotor was approximately 6.5 percent greater than that of the 20 or 30-bladed rotors. With a thrust-to-weight ratio of 1.62, a single 26-

bladed CFF rotor would be able to provide VTOL capabilities for a UAV with a light carbon fiber frame. However, the UAV payload would be severely limited with only a single CFF. Multiple CFFs could be used on a single UAV platform to not only provide a VTOL capability, but also allow for a substantial payload.

C. RECOMMENDATIONS

Several things could be done to improve future CFF analytical models. This study used one degree per time step in each ANYSYS CFX simulation, but the resolution would increase if a smaller time step is used in order to capture all of the perturbations in the flow. A thrust simulation was done for 30-bladed rotor at 7,000 RPM using a resolution of 0.5 degrees per time step and compared to the original simulation done at 1 degree per time step in Figure 33.

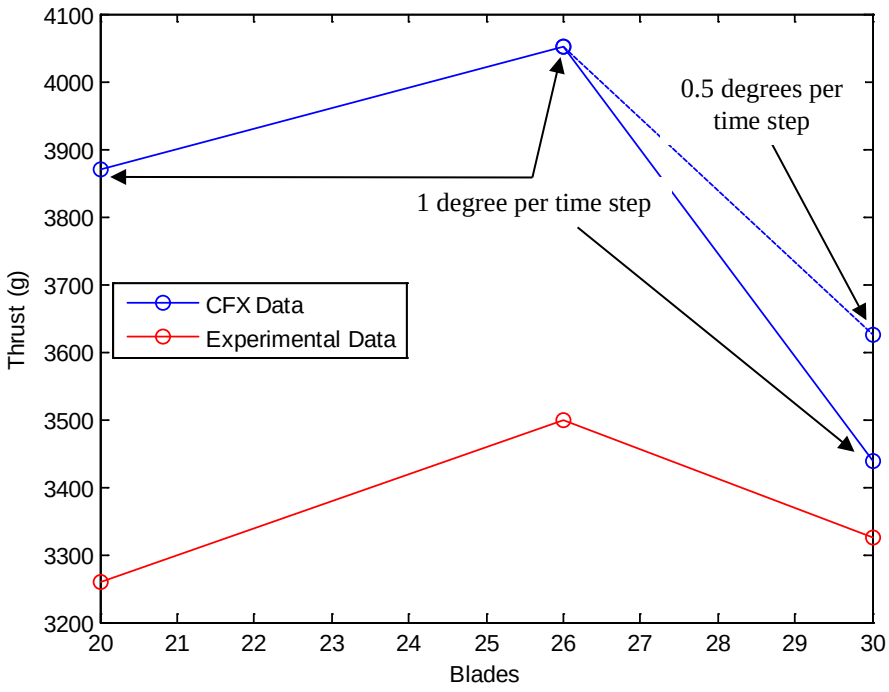

Figure 33. Thrust as a function of blade count with different time steps.

The predicted thrust for the 30-bladed rotor increased from the 3,437 g to 3,626 g, which is a 5.5 percent increase from the original model. Power calculations were also done with this improved resolution, which is shown in Figure 34.

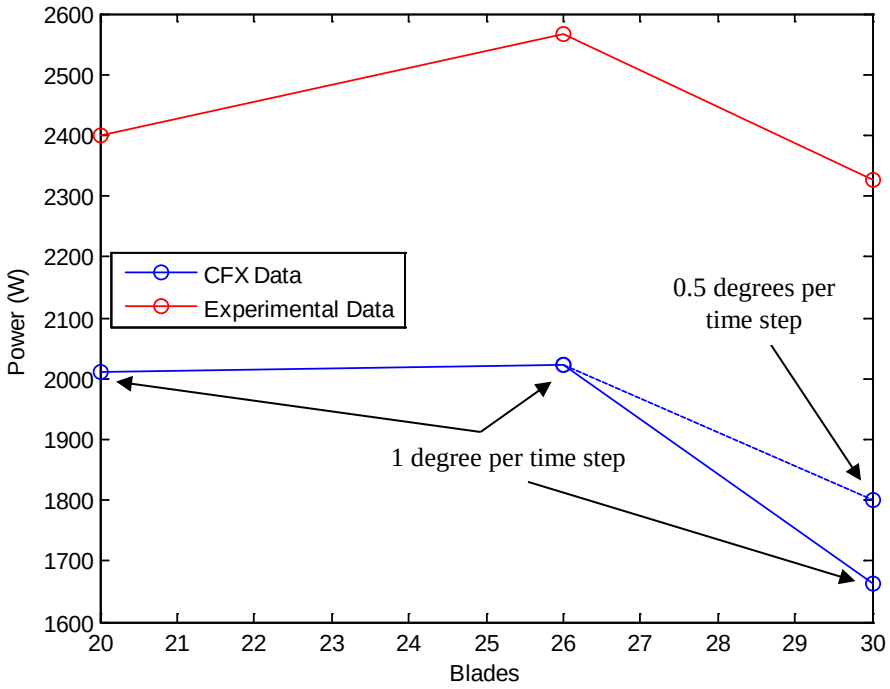

Figure 34. Power as a function of blade count with different time steps.

The power calculated with the improved time step is 1,800 W, which is an 8.2 percent increase when compared with the original analytical power value of 1,664 W. Both the power and thrust values are significantly increased when the resolution is improved, but the time to run each simulation also increases linearly with the reduction in time step.

In addition to changing the time step for the analytical simulation, the equation used to calculate the thrust in ANSYS CFX could also be changed. The velocity and mass flow rate variables in Equation (1) were mass averaged values across the entire outlet,

which produce an adequate thrust value for optimizing the number of blades on a rotor. However, the accuracy of these thrust calculations would be improved if Equation (4) were used.

$$T = \sum_{i=1}^{n} (\rho_i V_i^2 A_i) \quad (4)$$

In Equation (4) the density, the square of the exit velocity in the X-direction, and the element area are multiplied together at each individual element and then added. Equation (4) is represented by the expression "(sum(Density*Velocity u*Velocity u)@Outlet)*(0.0005[m]*0.001[m])" in the ANYSYS CFX expression editor. The area term is factored out of the summation because each element has the same area at the outlet. This equation would calculate a more accurate thrust value because it calculates the thrust at each element and adds them as opposed to a simple mass average of variables at the outlet.

The type of analysis could also be changed to increase the computational accuracy. A k-Epsilon turbulence model was used in this study, but Jones did both a k-Epsilon turbulence model and a laminar, unsteady flow model and compared the two results. She saw a 5.3 percent increase in thrust and a 38.9 percent increase in power when using the laminar, unsteady flow model instead of the k-Epsilon turbulence model [6].

Future studies can incorporate the optimized 4-inch rotor with 26 blades into a UAV, which has been previously been done for smaller rotors. Jones integrated four different CFFs, each with a 20-bladed rotor that was 3 inches in diameter, into a single UAV with a carbon fiber chassis [6]. The UAV, which was completely self-contained except wires running to the speed control console, was able to perform a vertical take-off. Integrating the larger, 4-inch rotors into a similar design will provide more thrust to the UAV and significantly increase the payload capacity.

APPENDIX A. CFF COMPONENT DRAWINGS

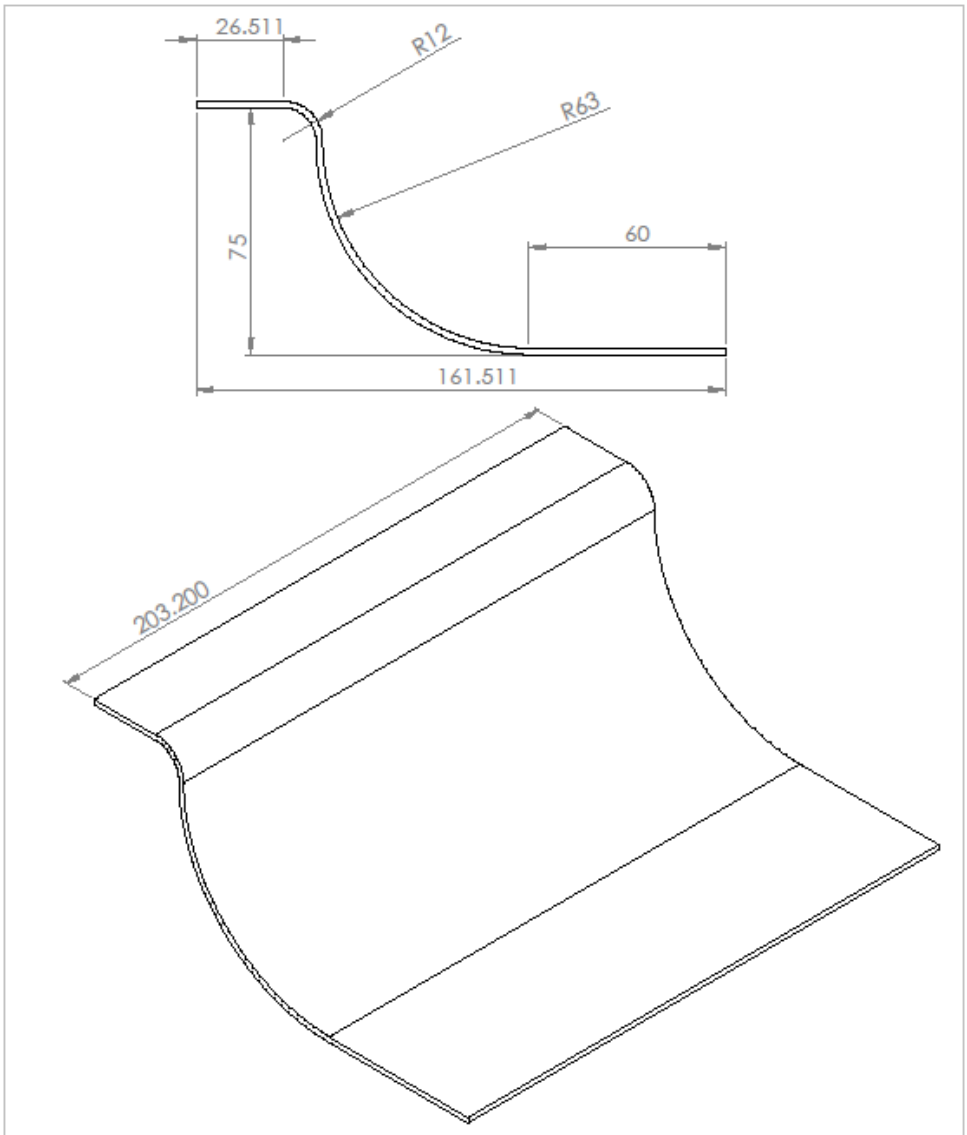

UNLESS OTHERWISE SPECIFIED: DIMENSIONS ARE IN MILLIMETERS SURFACE FINISH: TOLERANCES: LINEAR: ANGULAR:			FINISH:			DEBUR AND BREAK SHARP EDGES	DO NOT SCALE DRAWING / REVISION
							DIMENSIONS ARE IN MILLIMETERS
	NAME	SIGNATURE	DATE				TITLE:
DRAWN							
CHK'D							
APPV'D							
MFG							
Q.A				MATERIAL:			DWG NO. Lower Housing / A4
				WEIGHT:			SCALE:1:1.5 / SHEET 1 OF 1

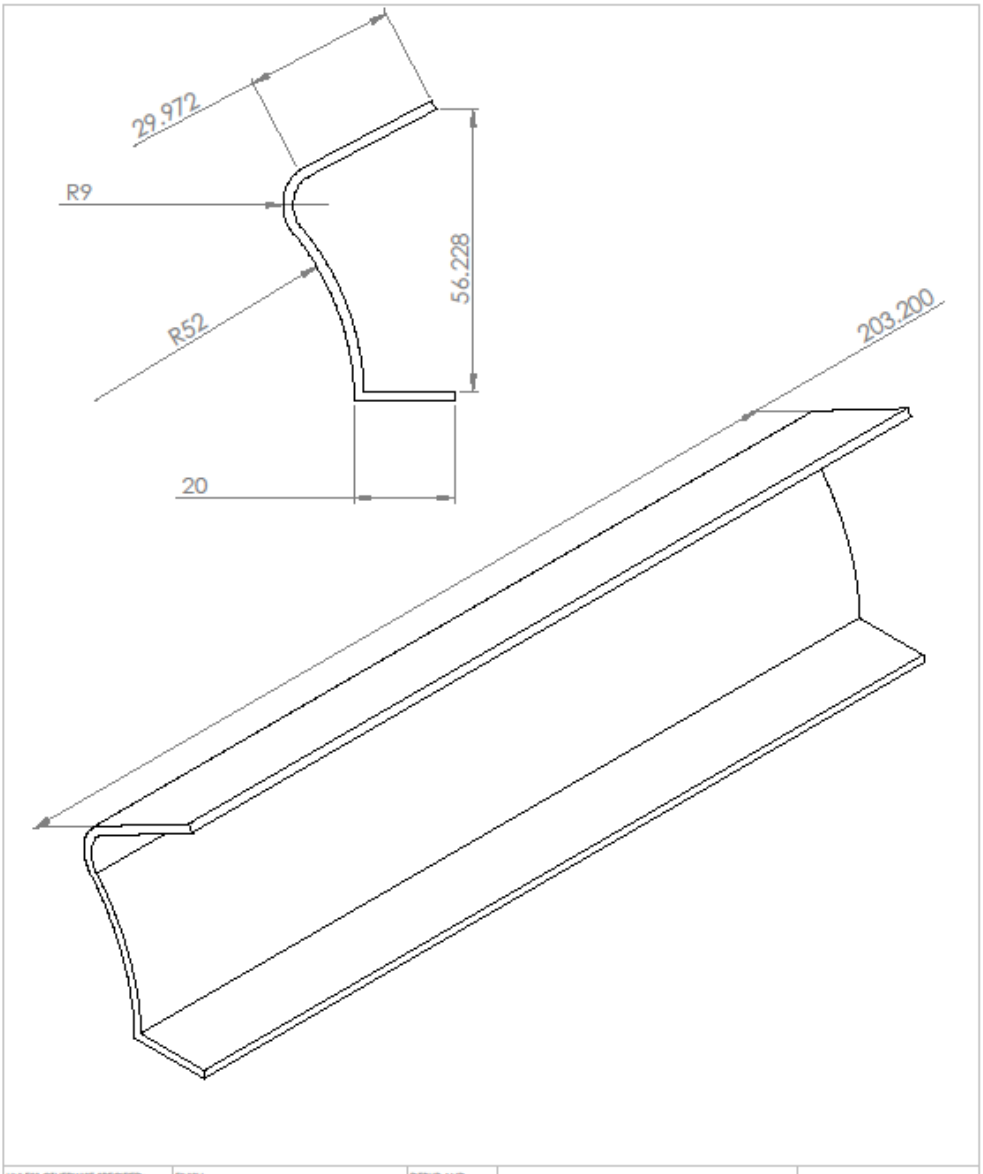

UNLESS OTHERWISE SPECIFIED: DIMENSIONS ARE IN MILLIMETERS SURFACE FINISH: TOLERANCES: LINEAR: ANGULAR:				FINISH:			DEBUR AND BREAK SHARP EDGES	DO NOT SCALE DRAWING	REVISION
								DIMENSIONS ARE IN MILLIMETERS	
	NAME	SIGNATURE	DATE					TITLE:	
DRAWN									
CHK'D									
APPV'D									
MFG									
Q.A				MATERIAL:				DWG NO. Upper Housing	A4
				WEIGHT:				SCALE:1:1	SHEET 1 OF 1

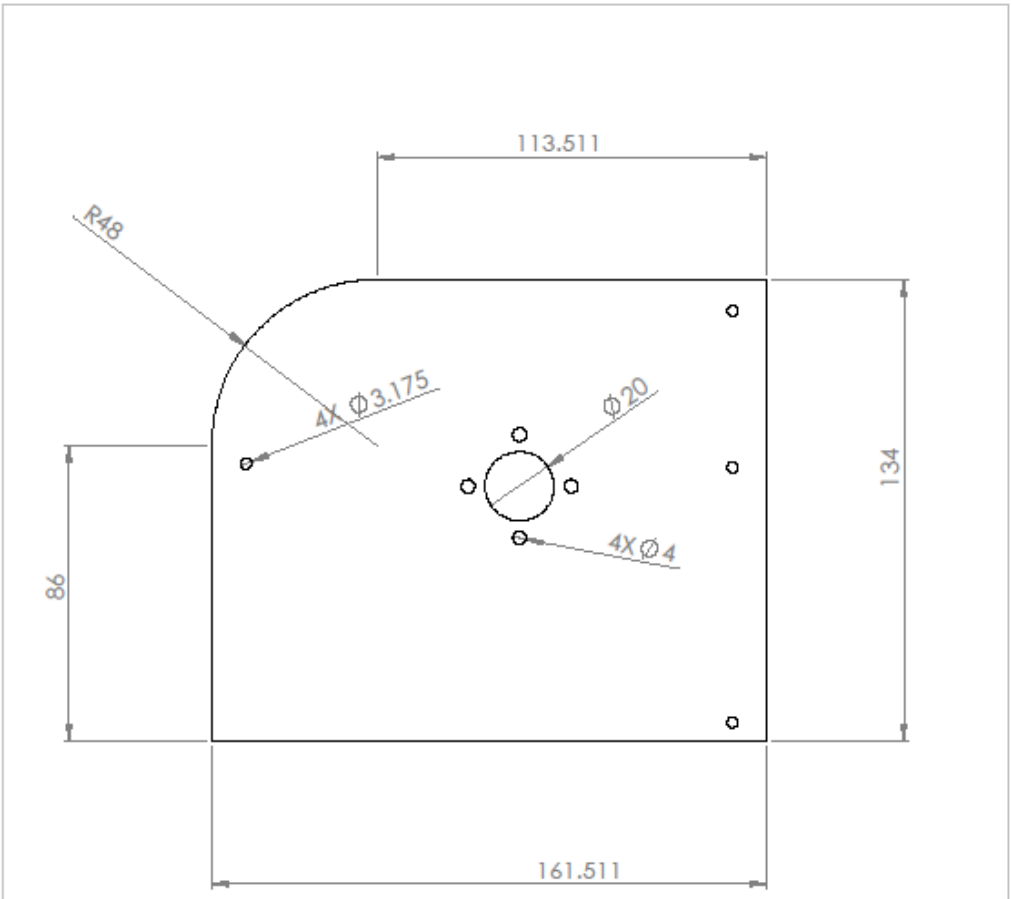

UNLESS OTHERWISE SPECIFIED: DIMENSIONS ARE IN MILLIMETERS SURFACE FINISH: TOLERANCES: LINEAR: ANGULAR:		FINISH:			DEBUR AND BREAK SHARP EDGES		DO NOT SCALE DRAWING	REVISION
							DIMENSIONS ARE IN MILLIMETERS	
	NAME	SIGNATURE	DATE				TITLE:	
DRAWN								
CHK'D								
APPV'D								
MFG								
Q.A				MATERIAL:			DWG NO. Endplate 1	A4
				WEIGHT:			SCALE:1:1.5	SHEET 1 OF 1

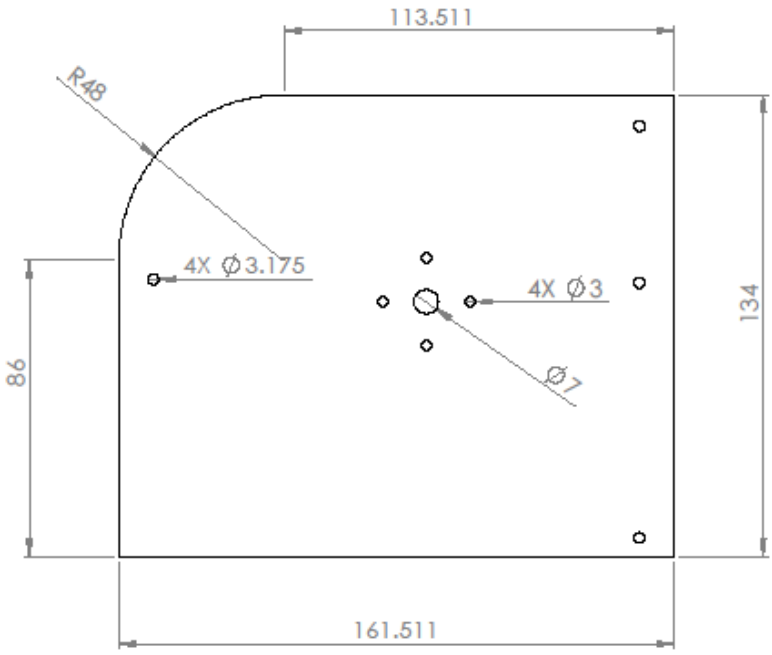

UNLESS OTHERWISE SPECIFIED: DIMENSIONS ARE IN MILLIMETERS SURFACE FINISH: TOLERANCES: LINEAR: ANGULAR:		FINISH:			DEBUR AND BREAK SHARP EDGES		DO NOT SCALE DRAWING	REVISION
							DIMENSIONS ARE IN MILLIMETERS	
	NAME	SIGNATURE	DATE				TITLE:	
DRAWN								
CHK'D								
APPV'D								
MFG								
Q.A				MATERIAL:			DWG NO. Endplate 2	A4
				WEIGHT:			SCALE:1:1.5	SHEET 1 OF 1

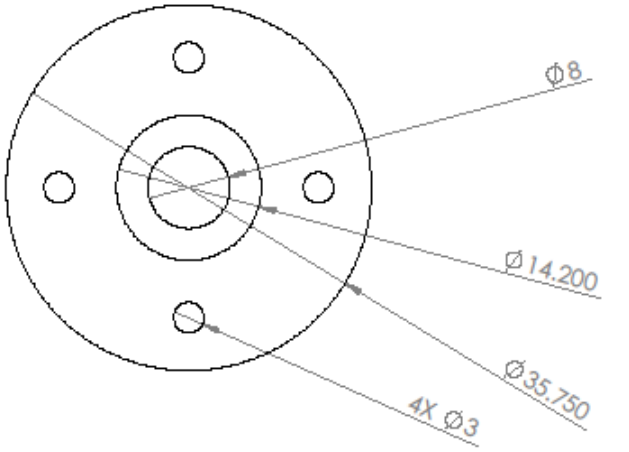

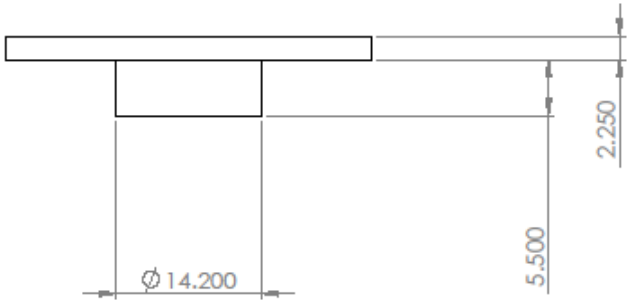

UNLESS OTHERWISE SPECIFIED: DIMENSIONS ARE IN MILLIMETERS SURFACE FINISH: TOLERANCES: LINEAR: ANGULAR:			FINISH:			DEBUR AND BREAK SHARP EDGES	DO NOT SCALE DRAWING / REVISION
	NAME	SIGNATURE	DATE				DIMENSIONS ARE IN MILLIMETERS
DRAWN							TITLE:
CHK'D							
APPV'D							
MFG							
Q.A				MATERIAL:			DWG NO. A3
							Housing Aluminum Bushing
				WEIGHT:			SCALE:2:1 / SHEET 1 OF 1

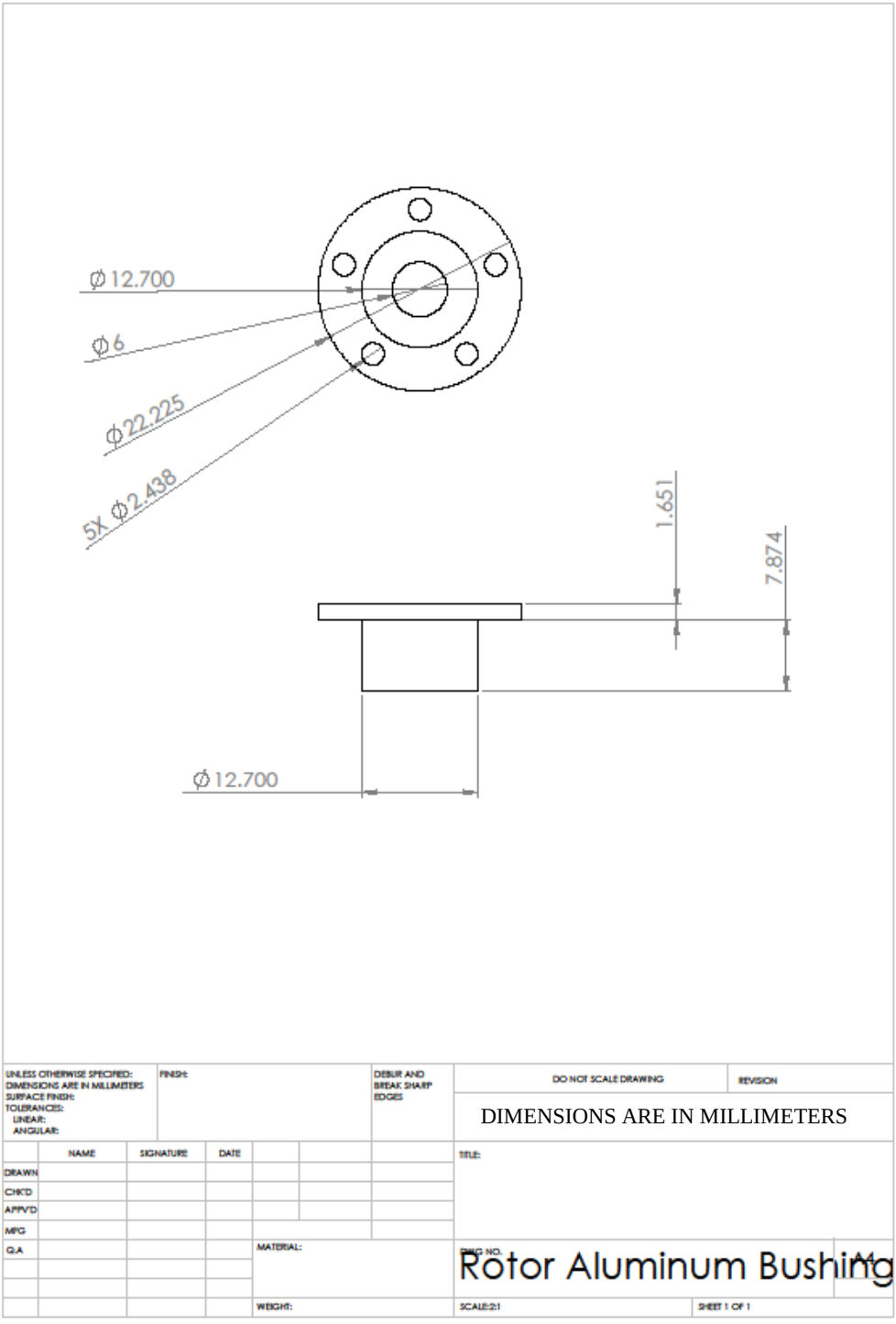
Ø12.700
Ø6
Ø22.225
5X Ø2.438
1.651
7.874
Ø12.700
UNLESS OTHERWISE SPECIFIED:
DIMENSIONS ARE IN MILLIMETERS
SURFACE FINISH:
TOLERANCES:
LINEAR:
ANGULAR:
FINISH:
DEBUR AND BREAK SHARP EDGES
DO NOT SCALE DRAWING
REVISION
DIMENSIONS ARE IN MILLIMETERS
NAME
SIGNATURE
DATE
DRAWN
CHK'D
APPV'D
MFG
Q.A
MATERIAL:
WEIGHT:
TITLE:
DWG NO.
Rotor Aluminum Bushing
A4
SCALE:2:1
SHEET 1 OF 1

APPENDIX B. ANSYS CFX SETTINGS FOR 26-BLADED ROTOR AT 7000 RPM

If property is excluded in the settings, it is unchecked.

Analysis

1. Analysis Type
    a. Basic Settings
        i. External Solver Coupling
            1. Option: None
        ii. Analysis Type
            1. Option: Transient
        iii. Time Duration
            1. Option: Total Time
            2. Total Time: 0.043 [s]
        iv. Time Steps
            1. Option: Timesteps
            2. Timesteps: 2.381e-005 [s]
        v. Initial Time
            1. Option: Automatic with Value
            2. 0 [s]

Housing Domain

1. Housing
    a. Basic Settings
        i. Location: B668
        ii. Domain Type: Fluid Domain
        iii. Coordinate Frame: Coord 0
        iv. Fluid and Particle Definitions…: Fluid 1
            1. Fluid 1
                a. Option: Material Library
                b. Material: Air Ideal Gas
                c. Morphology
                    i. Option: Continuous Flow
            2. Domain Models
                a. Pressure
                    ii. Reference Pressure: 1 [atm]
                b. Buoyancy Model
                    iii. Option: Non Buoyant
                c. Domain Motion
                    iv. Option: Stationary
                d. Mesh Deformation
                    v. Option: None

b. Fluid Models
    i. Heat Transfer
        1. Option: Total Energy
        2. Incl. Viscous Work Term: Checked
    ii. Turbulence
        1. Option: k-Epsilon
        2. Wall Function: Scalable
    iii. Combustion
        1. Option: None
    iv. Thermal Radiation
        1. Option: None
c. Initialization
    i. Domain Initialization: checked
    ii. Initial Conditions
        1. Velocity Type: Cylindrical
        2. Cylindrical Velocity Components
            a. Option: Automatic with Value
            b. Axial Component: 0 [m s^-1]
            c. Radial Component: 0 [m s^-1]
            d. Theta Component: 0 [m s^-1]
            e. Axis Definition
                vi. Option: Coordinate Axis
                vii. Rotation Axis: Global Z
            f. Static Pressure
                viii. Option: Automatic with Value
                ix. Relative Pressure: 1 [Pa]
            g. Temperature
                x. Option: Automatic with Value
                xi. Temperature: 288.15 [K]
            h. Turbulence
                xii. Option: Medium (Intensity = 5%)

2. Housing Default
    a. Basic Settings
        i. Boundary Type: Wall
        ii. Location: (automatically fills in)
    b. Boundary Details
        i. Mass and Momentum
            1. Option: No Slip Wall
        ii. Wall Roughness
            1. Option: Smooth Wall
        iii. Heat Transfer:
            1. Option: Adiabatic

3. HousingtoRotor1
    a. Basic Settings
        i. Boundary Type: Interface
        ii. Location: HousingInterface
    b. Boundary Details
        i. Mass and Momentum
            1. Option: Conservative Interface Flux
        ii. Turbulence
            1. Option: Conservative Interface Flux
        iii. Heat Transfer:
            1. Option: Conservative Interface Flux
4. Inlet
    a. Basic Settings
        i. Boundary Type: Opening
        ii. Location: Inlet
    b. Boundary Details
        i. Flow Regime
            1. Option: Subsonic
        ii. Mass and Momentum
            1. Option: Opening Pres. And Dirn
            2. Relative Pressure: 0 [Pa]
        iii. Flow Direction
            1. Option: Normal to Boundary Condition
        iv. Turbulence
            1. Option: Medium (Intensity = 5%)
        v. Heat Transfer:
            1. Option: Static Temperature
            2. Static Temperature: 288.15 [k]
5. Outlet
    a. Basic Settings
        i. Boundary Type: Outlet
        ii. Location: Outlet
    b. Boundary Details
        i. Flow Regime
            1. Option: Subsonic
        ii. Mass and Momentum
            1. Option: Average Static pressure
            2. Relative Pressure: 0 [Pa]
            3. Pres. Profile Blend: 0.05
        iii. Pressure Averaging:
            1. Option: Average Over Whole Outlet
6. Symmetry 1
    a. Basic Settings
        i. Boundary Type: Symmetry
        ii. Location: sym1,sym2

Rotor Domain

1. Rotor
    a. Basic Settings
        i. Location: B379
        ii. Domain Type: Fluid Domain
        iii. Coordinate Frame: Coord 0
        iv. Fluid and Particle Definitions…: Fluid 1
            1. Fluid 1
                a. Option: Material Library
                b. Material: Air Ideal Gas
                c. Morphology
                    i. Option: Continuous Flow
            2. Domain Models
                a. Pressure
                    i. Reference Pressure: 1 [atm]
                b. Buoyancy Model
                    i. Option: Non Buoyant
                c. Domain Motion
                    i. Option: Rotating
                    ii. Angular Velocity: 7000 [rev min^-1]
                    iii. Axis Definition
                        1. Option: Coordinate Axis
                        2. Rotation Axis: Global Z
                d. Mesh Deformation
                    i. Option: None
    b. Fluid Models
        i. Heat Transfer
            1. Option: Total Energy
            2. Incl. Viscous Work Term: Checked
        ii. Turbulence
            1. Option: k-Epsilon
            2. Wall Function: Scalable
        iii. Combustion
            1. Option: None
        iv. Thermal Radiation
            1. Option: None
    c. Initialization
        i. Domain Initialization: checked
        ii. Initial Conditions
            1. Velocity Type: Cylindrical
            2. Cylindrical Velocity Components
                a. Option: Automatic with Value
                b. Axial Component: 0 [m s^-1]
                c. Radial Component: 0 [m s^-1]
                d. Theta Component: 0 [m s^-1]

e. Axis Definition
    i. Option: Coordinate Axis
    ii. Rotation Axis: Global Z
f. Static Pressure
    i. Option: Automatic with Value
    ii. Relative Pressure: 1 [Pa]
g. Temperature
    i. Option: Automatic with Value
    ii. Temperature: 288.15 [K]
h. Turbulence
    i. Option: Medium (Intensity = 5%)

2. HousingtoRotor2
    a. Basic Settings
        i. Boundary Type: Interface
        ii. Location: RotorInterface
    b. Boundary Details
        i. Mass and Momentum
            1. Option: Conservative Interface Flux
        ii. Turbulence
            1. Option: Conservative Interface Flux
        iii. Heat Transfer:
            1. Option: Conservative Interface Flux
3. Rotor Default
    a. Basic Settings
        i. Boundary Type: Wall
        ii. Location: (automatically fills in)
        iii. Frame Type: Rotating
    b. Boundary Details
        i. Mass and Momentum
            1. Option: No Slip Wall
        ii. Wall Roughness
            1. Option: Smooth Wall
        iii. Heat Transfer:
            1. Option: Adiabatic
4. Symmetry 2
    a. Basic Settings
        i. Boundary Type: Symmetry
        ii. Location: sym3,sym4

Interface

1. Housing to Rotor
    a. Basic Settings
        i. Interface Type: Fluid Fluid
        ii. Interface Side 1
            1. Domain (Filter): Housing

2. Region List: HousingInterface
iii. Interface Side 2
1. Domain (Filter): Rotor
2. Region List: RotorInterface
iv. Interface Models
1. Option: General Connection
2. Frame Change/Mixing Model
a. Option: Transient Rotor Stator
3. Pitch Change
a. Option: Automatic
b. Additional Interface Models
i. Mass and Momentum
1. Option: Conservative Interface Flux
a. Interface Model
i. Option: None
c. Mesh Connection
i. Mesh Connection Method
1. Mesh Connection
a. Option: GGI

Solver

1. Solution Units
a. Basic Settings
i. Mass Units: [kg]
ii. Length Units: [m]
iii. Time Units: [s]
iv. Temperature Units: [K]
v. Angle Units: checked
1. Angle Units: [rad]
vi. Solid Angle Units: checked
1. Solid Angle Units: [sr]
2. Solver Control:
a. Basic Settings
i. Advection Scheme
1. Option: High Resolution
ii. Transient Scheme
1. Option: Second Order Backward Euler
2. Timestep Initialization
a. Option: Automatic
iii. Turbulence Numerics
1. Option: First Order
iv. Convergence Control
1. Min. Coeff. Loops: 1
2. Max. Coeff. Loops: 3
3. Fluid Timescale Control
a. Timescale Control: Coefficient Loops

4. Convergence Criteria
    a. Residual Type: RMS
    b. Residual Target: 1.E-4
b. Advanced Options
    i. Compressibility Control: Checked
        1. High Speed Numerics: Checked
3. Output Control
    a. Results
        i. Option: Standard
        ii. File Compression: Default
    b. Monitor
        i. Monitor Objects: Checked
            1. Monitor Points and Expressions
                a. Massflow_inlet: massFlow()@Inlet
                b. Massflow_outlet: massFlow()@Outlet
                c. Massflow_delta: massFlow()@Inlet+massFlow()@Outlet
                d. Rotor Torque: torque_z()@Rotor Default

THIS PAGE INTENTIONALLY LEFT BLANK

LIST OF REFERENCES

[1] J. D. Kummer and T. Q. Dang, "High-lift propulsive airfoil with integrated crossflow fan." *American Institute of Aeronautics and Astronautics*, vol. 43, pp. 1059–1068, Jul–Aug. 2006.

[2] J. Kummer, "Propulsive wing" [Online]. Available: www.propulsivewing.com (accessed May 1, 2013).

[3] C. T. Delagrange, "Viability of cross-flow fan for vertical take-off and landing aircraft," M.S. thesis, Department of Mechanical and Aerospace Engineering, Naval Postgraduate School, Monterey, CA, 2012.

[4] H. T. Yu, "Experimental investigation and numerical prediction of a cross-flow fan," M.S. thesis, Department of Mechanical and Astronautical Engineering, Naval Postgraduate School, Monterey, CA, 2006.

[5] Scorpion Precision Industry, "Scorpion Power System," [Online]. Available: www.scorpionsystem.com/catalog/motors/hk50/hk_5035_410/ (accessed May 8, 2013).

[6] A. M. Jones, "Integration of twenty-bladed cross-flow fan into vertical take-off and landing aircraft," M.S. thesis, Department of Mechanical and Aerospace Engineering, Naval Postgraduate School, Monterey, CA, 2013.

THIS PAGE INTENTIONALLY LEFT BLANK

INITIAL DISTRIBUTION LIST

1. Defense Technical Information Center
   Ft. Belvoir, Virginia

2. Dudley Knox Library
   Naval Postgraduate School
   Monterey, California